PINSA, **66, A**, No. 1, January 2000, pp. 137-175
© Printed in India

RESONANCE RAMAN INTENSITY ANALYSIS APPLIED TO PHOTODISSOCIATION REACTIONS OF POLYATOMIC MOLECULES

DAVID LEE PHILLIPS*

Department of Chemistry, University of Hong Kong, Pokfulam Road, Hong Kong

(Received 14 July 1999; Accepted 09 September 1999)

We present several applications of resonance Raman intensity analysis to the investigation of direct photodissociation reactions in polyatomic haloalkane molecules. Our studies show that direct C-I bond cleavage in polyatomic iodoalkanes and other haloalkanes have multidimensional reaction coordinates that appear to be qualitatively consistent with impulsive "semi-rigid"radical descriptions of the photodissociation dynamics. We also find that the initial photodissociation dynamics show interesting correlation with trends observed in the results of energy partitioning to the reaction products as determined by time-of-flight photofragment spectroscopy experiments. Comparison of gas and solution phase short-time photodissociation dynamics shows that they are generally very similar in the Franck-Condon region of the reaction but can be significantly different in the case where symmetry breaking occurs such as in the diiodomethane molecular system. We have examined several examples of bond selective electronic excitation in dihalomethane and dihaloethane molecules and have found that the short-time photodissociation dynamics show some correlation with the degree of interaction between the two carbon-halogen chromophores and we discuss the implications for bond selective photochemistry and energy partitioning.

Key Words: Raman Spectroscopy; Photodissociation; Chemical Dynamics; Iodoalkanes; Haloalkanes

Introduction

This review article will focus on using resonance Raman intensity analysis to examine the Franck-Condon region of molecular electronic excited states associated with direct photodissociation reactions. This article is not intended to be comprehensive on either resonance Raman intensity analysis or direct photodissociation reactions, but is meant to provide a range of examples of the applications of resonance Raman intensity analysis to direct photodissociation reactions. There are several excellent reviews on the general aspects of resonance Raman intensity analysis and the reader is referred to these for more details and a broader understanding of this topic.[1-8] Examples of molecular systems studied by the author in the laboratory over the past six years have been stated in this article alongwith a number of other selected applications. For the purpose of this review article, a focus on haloalkane molecular systems have been given since they were extensively studied as examples and prototypes for understanding direct photodissociation reactions.

Haloalkanes and in particular the A-band photodissociation reactions of iodoalkanes have been intensely studied as model molecular systems for better understanding direct photodissociation reactions. The A-band absorption spectra of gas and solution phase iodoalkanes are smooth and featureless. They are composed of three transitions ($^3Q_0$, $^1Q_1$, and $^3Q_1$) of which the $^3Q_0$ transition accounts for most of the oscillator strength and correlates with production of I* photofragments.[9-11] Ground electronic state iodine atoms (I) may be produced in significant amounts due to an electronic non-adiabatic curve-crossing of the $^3Q_0$ state by the $^1Q_1$ state.[12-19] Photofragment anisotropy measurements from molecular beam experiments have demonstrated that the direct C-I bond breaking process occurs much faster than the rotational period of the parent molecule.[19-26]

Iodomethane has been by far the most intensively examined A-band photodissociation reaction for iodoalkane molecules. Magnetic

*E-mail: Phillips@HKUCC.HKU.HK, Fax: 852-2857-1586

circular dichroism (MCD) measurements have shown that the $^3Q_0$ transition located near the center of the A-band absorption has approximately 70-80% of the total oscillator strength with the $^3Q_1$ and $^1Q_1$ near the red and blue edges of the absorption having the rest of the oscillator stength.[10] High resolution time-of-flight photofragment spectroscopy experiments displayed noticeable internal energy in the umbrella mode vibration of the methyl radical photofragment.[20,21] Several different techniques such as multiphoton ionization (MPI), coherent anti-Stokes Raman scattering (CARS), diode laser absorption, and others have been used to measure the vibrational and rotational state distributions of the methyl radical photofragments produced from the A-band photodissociation reaction.[27-32] The iodomethane A-band photodissociation reaction time has been directly measured using femtosecond time-resolved pump-probe experiments.[33,34] Different potential energy surfaces and theoretical models with differing degrees of complexity have been used to simulate the A-band photodissociation reaction of iodoalkanes.[35-44] Much of the experimental data available for iodomethane has been simulated using fully quantum mechanical calculations with fairly accurate *ab initio* potential energy surfaces.[43,44] Thus, the major aspects of the A-band photodissociation reaction of iodomethane have been elucidated.

The A-band photodissociation reactions of larger iodoalkanes as well as dihaloalkanes have not been nearly as intensively investigated as has iodomethane. Inspection of larger haloalkanes allow one to examine how the molecular structure and substituents change the photodissociation dynamics, energy partitioning to the photofragments and the probability of $^3Q_0$ to $^1Q_1$ curve crossing. Time-of-flight translational spectroscopy experiments carried out for several larger iodoalkanes have shown that as the alkyl group becomes more massive and/or more branched in structure then the amount of internal excitation of the alkyl radical photofragment increases.[19-26,45-53] A variety of experimental determinations of the I*/I ratio as a function of the structure and mass of the parent iodoalkane demonstrated that more I photofragment is produced as the iodoalkane molecule becomes more massive or more branched in structure.[12-19,54-61] These results imply that the $^3Q_0$ to $^1Q_1$ curve crossing probability has a degree of dependence on the amount of internal energy imparted to the alkyl photofragment: less of the available energy of the photodissociation reaction is imparted into translational of the two photofragments as more of the available energy is partitioned to internal excitation of the alkyl photofragment and this leads to an increase in the curve crossing probability.

The energy partitioning associated with A-band iodoalkane photodissociation reactions have been interpreted in terms of two simple models for the photodissociation dynamics of direct bond breaking reactions.[20,23-25] One model called the "rigid radical" model assumes that the alkyl radical maintains the same structure during the photodissociation and this results in only internal excitation of the rotational degree of freedom for the alkyl radical. The other model called the "soft radical" model assumes that the α-carbon atom is very loosely linked to the rest of the alkyl radical which results in the α-carbon atom being shoved into the rest of the radical during the C-I bond breaking and this gives rise to internal excitation of both vibrational and rotational degrees of freedom. Both the "rigid radical" and "soft radical" models of the photodissociation dynamics do not realistically describe the α-carbon atom bonding to the rest of the radical during the photodissociation reaction. In the "rigid radical" model the α-carbon atom is too strongly bonded to the rest of the radical in order to maintain a rigid alkyl radical structure during the photodissociation. However, in the "soft radical" model the α-carbon atom is too weakly bonded to the rest of the alkyl radical during the photodissociation reaction. The energy disposal observed for most iodoalkane molecular systems examined so far are somewhere between the results predicted by the "rigid radical" and "soft radical" models although most experimental results are closer to the values of the "soft radical" model.[20,23-25] More accurate and realistic models for direct photodissociation dynamics need to be developed to better describe the energy partitioning. In order to do this, it would be very helpful to examine the initial photodissociation dynamics at the vibrational-mode specific level. Resonance Raman spectroscopy can be used to investigate the initial or short-time photodissociation dynamics at the vibrational-mode specific level and provide an additional

experimental constraint on newly developed models of direct photodissociation reactions. In this review article results of several resonance Raman intensity analysis investigations done for selected haloalkane molecular systems have been presented. These resonance Raman studies examine how the initial or short-time photodissociation dynamics are influenced by substituents and molecular structure.

Experimental

A brief description of the experimental apparatus and methods to obtain resonance Raman spectra of photodissociating molecules[62-73] is now presented. Spectroscopic grade solvent (usually cyclohexane, methanol or acetonitrile) and the haloalkane under investigation were used to prepare samples for the solution phase resonance Raman experiments. Concentrations for the samples could vary from 0.05 to 0.3 M depending on the strength of the A-band absorption. The harmonics of a nanosecond Nd:YAG laser and their hydrogen Raman shifted laser lines provided the excitation wavelengths for the resonance Raman experiments. Typically, the excitation laser used 50 to 100 μj loosely focused to a 1 mm diameter on the flowing liquid stream of sample. A backscattering geometry was used to collect the Raman scattered light from the excited portion of the flowing liquid sample. Reflective optics (an ellipsoidal mirror with f/1.4 and a flat mirror) were used to collect the Raman light and image it through a depolariser and the entrance slits of a 0.5 metre spectrograph. The 1200 groove/mm grating of the spectrograph dispersed the Raman scattered light onto a liquid nitrogen cooled CCD detector mounted on the exit port of the spectrograph. The signal of the CCD was acquired from 60 to 600 s before being read out from the CCD detector to an interfaced PC computer. The summation of ten to thirty of these readouts gave the resonance Raman spectrum.

The gas phase resonance Raman experiments used the same excitation source, collection optics, and detection equipment as the solution phase experiments. The gas phase sample handing apparatus was composed of a heated reservoir of liquid and vapour haloalkane connected to a heated pipette. Dry nitrogen was flowed through this sample reservoir to take away some of the haloalkane vapour with it out through the pipette nozzle. The excitation laser beam was loosely focused near the exit of the pipette nozzle. An approximate 90 degree geometry was used for collection of the Raman scattered light using the reflective optics. So as to avoid interference from photoproduct bands, the excitation laser power was kept fairly low (typically < 100 μj over a 2 mm beam diameter). The excitation laser light was not noticeably attenuated by the vapour haloalkane sample in the gas phase experiments and the sample reabsorption of the resonance Raman scattering was minimal for the gas phase resonance Raman spectra.

The wavenumber Raman shifts of the resonance Raman spectra were calibrated by the known vibrational frequencies of the solvent for the solution phase spectra and the mercury emission lines as well as gas phase nitrogen and oxygen Raman bands for the gas phase spectra. The reabsorption of the Raman scattered light by the sample in the solution phase experiments was minimized by the backscattering geometry employed in the experiments. Any remaining sample reabsorption of the resonance Raman scattering in the solution phase spectra was corrected for by the methods described in ref. [74]. An appropriately scaled solvent spectrum was subtracted from the reabsorption corrected solution phase resonance Raman spectrum in order to eliminate the solvent Raman bands. The channel to channel variation of the entire detection apparatus was corrected for using a spectrum obtained of a calibrated intensity standard deuterium lamp and/or a calibrated intensity standard tungsten lamp. Portions of the corrected resonance Raman spectra were fitted to a base line plus a sum of Lorentzians to obtain the integrated areas of the Raman bands. Absolute Raman cross sections were determined using spectrophotometrically measured sample concentrations and previously measured absolute Raman cross sections for solvent bands[75,76] as an internal standard. For the experimental details associated with any particular molecular system, the reader is referred to the original publications.

Theory and Calculations

The theory and calculations used to simulate the experimental resonance Raman and absorption cross sections associated with the A-band photodissociation reactions of haloalkanes[62-73] are now described. We have used a relatively simple

model and time-dependent wavepacket calculations in order to extract the major features of the A-band haloalkane short-time photodissociation dynamics. The models and calculations that we use are not intended to be a complete description of the resonance Raman and absorption spectra, but are meant to provide a modest beginning to better understand the vibrational mode-specific dynamics of the initial bond cleavage process in A-band haloalkanes. The simulation results will also provide a useful reference to which more sophisticated computational results can be compared to assess the relative importance of effects like the possible Duschinsky rotation of normal coordinates, nonadiabatic curve crossings, possible coordinate dependence of the transition dipole moment, and others.

We generally use the following formula to simulate the A-band absorption spectra of haloalkanes:

$$\sigma_A(E_L) = (4\pi e^2 E_L M^2 / 3n\hbar^2 c) \sum_i P_i \, \mathrm{Re} \left[\int_0^\infty \langle i|i(t)\rangle \exp[i(E_L+\varepsilon_i)t/\hbar]\exp[-g(t)]\, dt \right] \quad \ldots (1)$$

The resonance Raman cross sections were computed from the following expression:

$$\sigma_{R,}(E_L, \omega_s) = \sum_i \sum_f P_i \, \sigma_{R,i\rightarrow f}(E_L) \, \delta(E_L + \varepsilon_i - E_S - \varepsilon_f)$$

with

$$\sigma_{R,i\rightarrow f}(E_L) = (8\pi e^4 E_S{}^3 E_L M^4 / 9\hbar^6 c^4) \left| \int_0^\infty \langle f|i(t)\rangle \exp[i(E_L+\varepsilon_i)t/\hbar] \exp[-g(t)]\, dt \right|^2 \quad \ldots (2)$$

where E_L is the incident photon energy, E_S is the scattered photon energy, M is the transition length evaluated at the equilibrium geometry, n is the solvent index of refraction, P_i is the initial Boltzmann population of the ground-state energy level $|i\rangle$ which has energy ε_i, f is the final state for the resonance Raman process, and ε_f is the energy of the ground state energy level $|f\rangle$. $\delta(E_L + \varepsilon_i - E_S - \varepsilon_f)$ is a delta function to sum cross sections with the same frequency and $|i(t)\rangle = e^{-iHt/\hbar}|i\rangle$ is $|i(t)\rangle$ propagated on the excited state surface for a time t where H is the excited state vibrational Hamiltonian. The $exp[-g(t)]$ term in eqs. (1) and (2) is a damping function which is usually expected for the directly photodissociating A-band haloalkanes to be mostly direct photodissociation population decay with some solvent dephasing for the solution phase reactions. Addition over a ground state Boltzmann distribution of vibrational energy levels (298 K temperature distribution) was usually used to compute the absorption and resonance Raman cross sections.

The ground and excited state potential energy surfaces were approximated by harmonic oscillators displaced by Δ in dimensionless normal coordinates. We assumed the Condon approximation (e.g. no coordinate dependence of the transition length). The resonance Raman intensities of the first several overtones and combination bands are determined mainly by the slope of the excited state surface in the Franck-Condon region when no vibrational recurrences take place as is the case for a direct photodissociation reaction. The gas and solution phase A-band absorption spectra of haloalkanes are typically structureless and this suggests that the total electronic dephasing is mostly due to direct photodissociation prior to the first vibrational recurrence time. The wavepacket propagation in the calculations was usually cut off after 30 or 40 fs in order not to allow any significant recurrences of the wavepacket to the Franck-Condon region. The $\langle f|i(t)\rangle$ overlaps decay and reach a negligible value after 20 to 30 fs for the resonance Raman bands observed in our experimental spectra for the haloalkanes we have examined so far. Thus, the cut-off at 30 to 40 fs only prevents the wavepacket to return to the Franck-Condon region and helps to better model the direct photodissociation reactions of A-band haloalkanes. For the solution phase studies, the effects of solvent dephasing collisions on the absorption and resonance Raman cross sections were modeled by an exponential decay (where the $exp[-g(t)]$ term in equations (1) and (2) was replaced by $\exp[-t\Gamma/\hbar]$). The bound harmonic oscillator model for the excited state used for our simulations of the A-band haloalkanes only provides us a convenient method to mimic the portion of the excited state that determines the resonance Raman intensities and absorption spectrum and does not imply the excited state is bound.

The potential parameters in equations (1) and (2) are typically given in terms of dimensionless normal coordinates. So as to easily visualize the short-time photodissociation dynamics in terms of bond length and bond angle changes, we converted the normal coordinate motions into internal coordinate motions. The center of the wavepacket motion undergoing separable harmonic dynamics

in terms of dimensionless normal coordinates at time t after photoexcitation to the excited state can be expressed by

$$q_\alpha(t) = \Delta_\alpha (1\text{-}cos\omega_\alpha t) \quad \ldots (3)$$

The time, t, is in units of fs and the vibrational frequency, ω_α, is in units of fs^{-1}. We fix $q_\alpha = 0$ for each mode α at the ground electronic state equilibrium geometry. At different times t the internal coordinate displacements are obtained from the dimensionless normal mode displacements ($q_\alpha(t)$) using the following formula:

$$s_i(t) = (h/2\pi c)^{1/2} \Sigma_\alpha A_{\alpha i} \varpi_\alpha^{-1/2} q_\alpha(t) \quad \ldots (4)$$

S_i are the displacements of the internal coordinates (bond stretches, bends, torsions, and wags as defined by Wilson, Decius, and Cross) from their ground electronic state equilibrium values. $A_{\alpha i}$ is the normal-mode coefficient ($\partial s_i/\partial Q_\alpha$) with Q_α = the ordinary dimensioned normal coordinate. ω_α is the vibrational frequency in units of cm^{-1}. For each of the haloalkane molecular systems that has been investigated, normal coordinate calculations have been done using a modified version of the Snyder and Schachtschneider FG program[77] and used either a previously reported force field to which small modifications were incorporated to better fit the experimental vibrational frequencies or a force field that has been derived. The results of these normal coordinate calculations were then used to compute the normal mode vectors for the haloalkane under investigation. For more detailed descriptions of the models and calculations used for any particular haloalkane, the reader is referred to the original publications associated with that particular haloalkane molecular system.

Results and Discussion

A. Iodomethane

There have been many resonance Raman and/or emission studies done for the A-band iodomethane direct photodissociation reaction. Brus and Bondybey[78] first examined the emission produced by iodomethane in low temperature matrices following A-band absorption photoexcitation and they observed many C-I stretch higher overtones. Kinsey and coworkers carried out the first resonance Raman experiments on the A-band photodissociation reaction of iodomethane in the gas phase.[79-81] Their initial resonance Raman experiments[79] published in 1984 showed a long overtone progression in the nominal C-I stretch mode ($n\nu_3$) with a small combination band progression of the methyl umbrella mode plus the C-I stretch overtones ($\nu_2+n\nu_3$). These spectra were consistent with a qualitative model of the photodissociation in which the C-I bond lengthens during the photodissociation and the CH_3I tetrahedral angles relax toward a planar CH_3 photofragment. The observed slow increase in the combination band progression of the methyl unmbrella mode plus the C-I stretch overtones ($\nu_2+n\nu_3$) relative to the C-I stretch overtones ($n\nu_3$) with an increase in n reflects the progressive preference for planar CH_3 geometries as the C-I bond becomes longer on the $^3Q_0$ potential energy surface. Kinsey and coworkers later carried out higher resolution studies on both CH_3I and CD_3I.[80] They also obtained detailed excitation profiles and depolarization ratio experiments for gas phase iodomethane.[81] Kinsey and coworkers found that the depolarization ratios of all of the Raman bands examined were close to one third which is the value expected for a parallel transition to one or more excited states.[81] They also found that the Raman excitation profiles for overtones and combination bands had simple smooth contours and could be fit well using the short-time theory of Raman scattering for motion on a single repulsive potential energy surface.[81] However, the C-I stretch fundamental Raman excitation profile had a bimodal shape and could be fit reasonably well using a model where the C-I stretch fundamental was perturbed by off resonant interference from a higher energy state or states with parallel transition character.[81] The next section discusses this type of resonant-preresonant interference in the Raman excitation profiles of fundamental bands.

Several other groups have also examined various aspects of the A-band iodomethane photodissociation reaction. Butler and coworkers[82] measured depolarization ratios of gas phase iodomethane for the C-I stretch overtones ($n\nu_3$) up to n=12. They found that while the fundamental and lower overtones had depolarization ratios close to one third, the higher overtone depolarization ratios progressively increased noticeably.[82] This behaviour was ascribed to effects of the amount of wavepacket sampling of the $^3Q_0$-$^1Q_1$ conical intersection.[82] However, a later study by Ziegler *et*

al.[83] using higher resolution and a different depolarization ratio measurement method found Raman depolarization ratios that disagree a bit with previous results by Butler and coworkers[82] as well as Kinsey and coworkers.[81] Ziegler and coworkers[83] did not find as strong a change in depolarization ratio with vibrational quantum number as did Butler and coworkers.[82] Ziegler and coworkers used the ratio of oscillator strengths of the $^3Q_0$ and $^1Q_1$ transitions found by the MCD measurements of Gedanken and Rowe and showed that their Raman depolarization ratios and rotational contours can be modeled reasonably well using interference due to two processes: parallel absorption followed by parallel emission ($^3Q_0$) and perpendicular absorption followed by perpendicular emission ($^1Q_1$).[83] This is somewhat different from the conclusions of Butler and coworkers[82] and Kinsey and coworkers.[81] Further work is needed to completely resolve the issue of how sensitive the iodomethane Raman depolarization ratios are to nonadiabatic interactions and/or how much direct excitation of the $^1Q_1$ transition contributes to the resonance Raman intensities.

Myers *et al.*[84-86] examined the solution phase resonance Raman spectra of iodomethane in several different solvents. The solution phase spectra were very similar to those in the gas phase and also exhibited most of their intensity in the C-I stretch overtone progression. Detailed comparison of the iodomethane spectrum in hexane solution with previous gas phase spectra showed the spectra were almost the same up to n= 9 of the C-I stretch overtone progression and very similar to one another up to n=16 (though the solution Raman band positions shifted slightly to lower frequency due to solvent-solute attractive interactions). The solution phase Raman band positions may shift slightly relative to the gas phase values due to the balance of attractive versus repulsive solvent-solute forces on the ground state potential energy surface. The solution phase resonance Raman relative intensities may change somewhat in the Franck-Condon region due to solvent effects on the excited state. However, the solution phase resonance Raman spectra of iodomethane are very similar to the corresponding gas phase spectra and indicate that the short-time photodissociation dynamics near the Franck-Condon geometries are very similar to one another.

Many theoretical models and potential energy surfaces have been developed and applied to the A-band photodissociation of iodomethane over the years.[35-44] These models and potential energy surfaces have become increasingly sophisticated and better able to model the experimental data available. Fully quantum mechanical simulations using fairly accurate *ab initio* potential energy surfaces were used to fit much of the available experimental data for iodomethane[43,44] and it appears the major features of the A-band photodissociation have been elucidated. However, there are still some aspects of the A-band photodissociation of iodomethane that need to be better understood such as the role of the $^1Q_1$ transition in the A-band absorption and resonance Raman spectra and nonadiabatic effects on the resonance Raman depolarization ratios. For a more complete discussion of the A-band photodissociation reaction of iodomethane and the interplay between theory and experiment in better understanding this reaction, the reader is referred to the excellent recent review article by Kinsey and coworkers.[6]

B. Higher Iodoalkanes: Effects of Mass and Branching of the Alkane Chain

Fig. 1 shows the absorption spectra of iodoethane, 2-iodopropane, and 2-methyl-2-iodopropane in cyclohexane solution. The excitation frequencies for the resonance Raman experiments are shown in nm above each absorption spectrum. All of the iodoalkanes have very similar A-band absorption spectra with a maximum near 260 nm and modest intensity.[87-90] The iodoalkanes also have a much larger B-band absorption ~196 nm due to transitions to a bound Rydberg state which predissociates to the lower purely repulsive electronic states.

Figs. 2-4 give an overview of the A-band and B-band resonance Raman spectra obtained for iodoethane, 2-iodopropane, and 2-methyl-2-iodopropane for the excitation wavelengths indicated in Fig. 1.[89] Fig. 5 presents an expanded view of the 258 nm A-band resonance Raman spectrum of iodoethane in cyclohexane solution. The spectra in Figs. 2-5 have been corrected for sample reabsorption of the Raman light, sensitivity corrected for the wavelength dependence of the detection system, and solvent subtracted. The subtraction of the very strong C-H bands of the

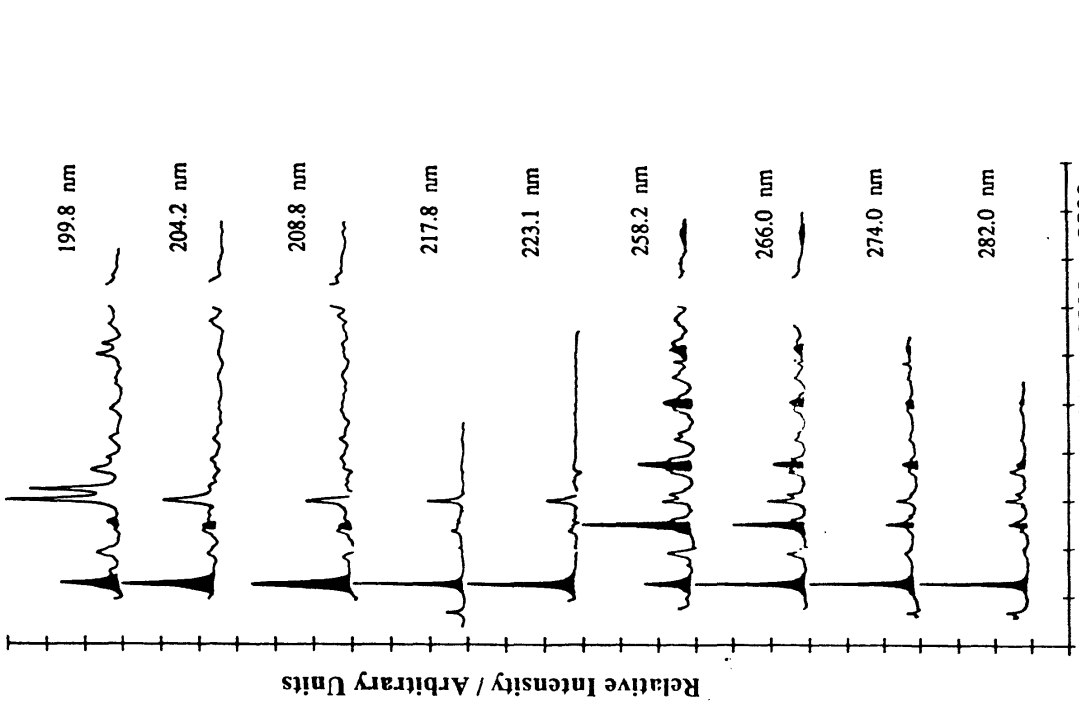

Fig. 2 Overview of the iodoethane resonance Raman spectra. The spectra are intensity corrected and solvent subtracted. The shaded bands in the spectra are the nominal C-I stretch progression. The CH stretch region is not shown because of a very big solvent subtraction artifact.

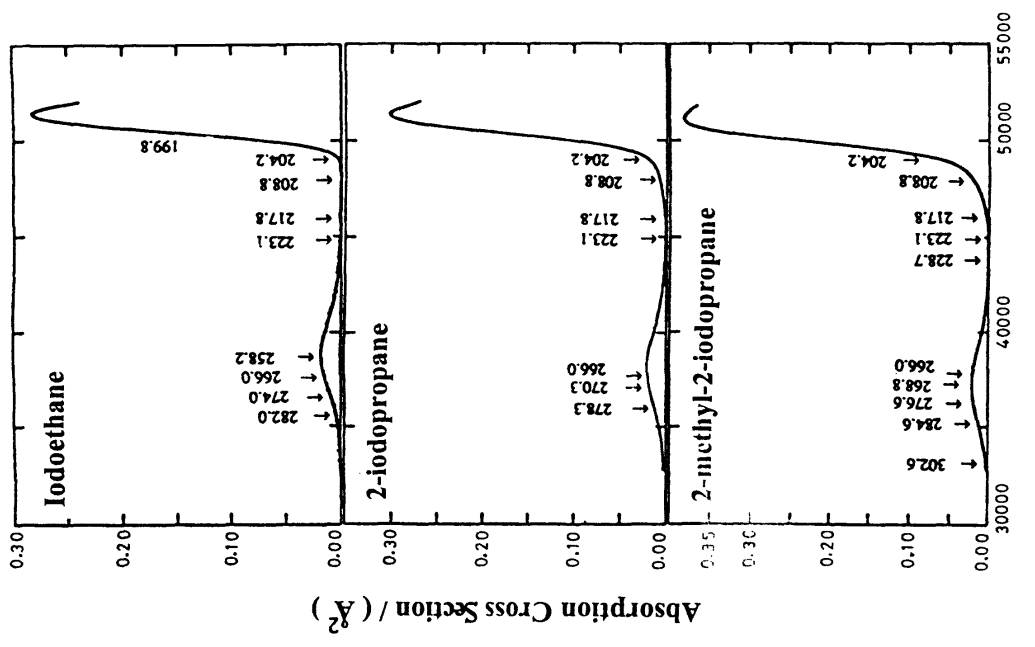

Fig. 1 Absorption spectra of iodoethane, 2-iodopropane, and 2-methyl-2-iodopropane in cyclohexane solution. The resonance Raman excitation frequencies are shown above each absorption spectrum. The A-band absorption is the weak band around 30,000 cm^{-1} to 45,000 cm^{-1}.

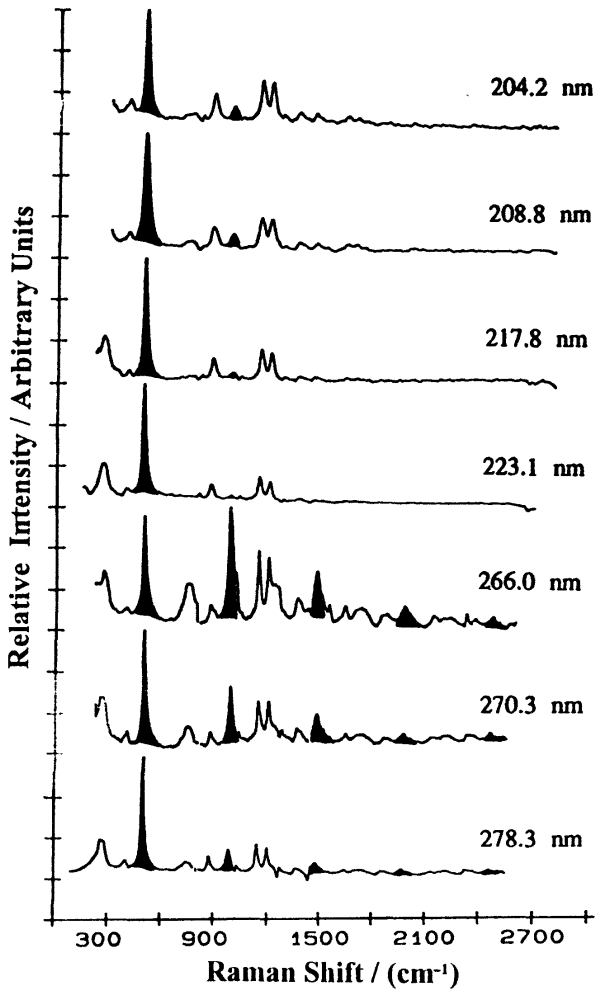

Fig. 3 Overview of the 2-iodopropane resonance Raman spectra. The spectra are intensity corrected and solvent subtracted. The shaded bands in the spectra are the nominal C-I stretch progression. The CH stretch region is not shown because of a very big solvent subtraction artifact.

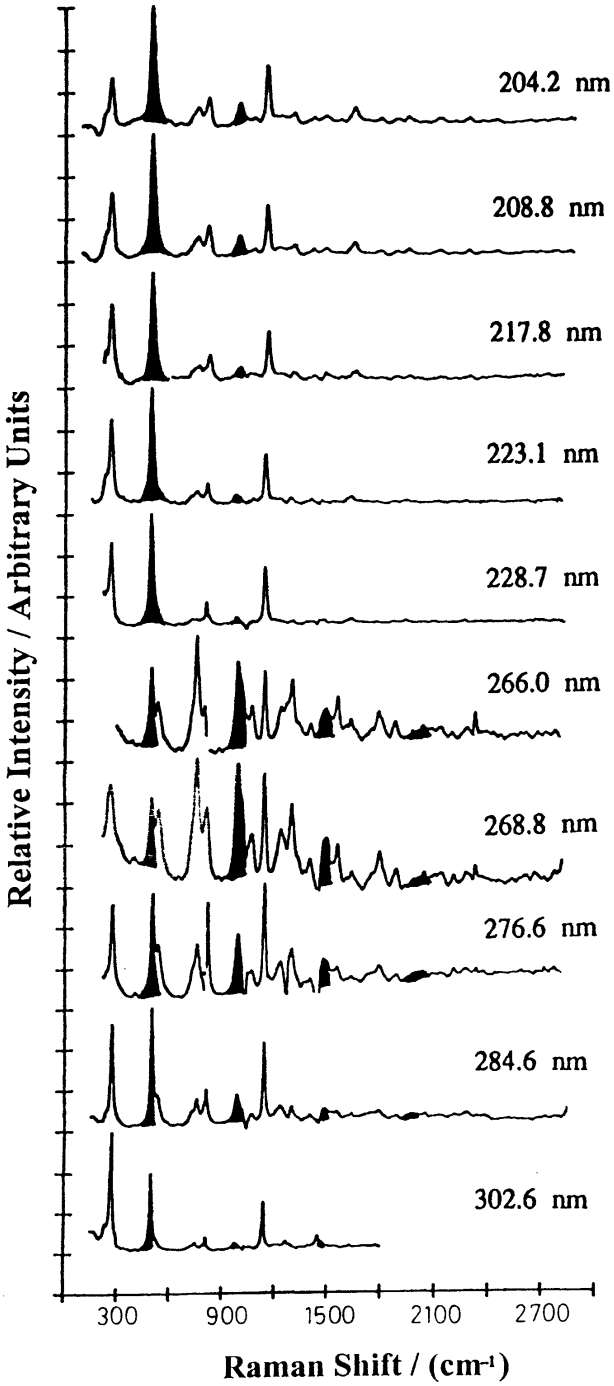

Fig. 4 Overview of the 2-methyl-2-iodopropane resonance Raman spectra. The spectra are intensity corrected and solvent subtracted. The shaded bands in the spectra are the nominal C-I stretch progression. The CH stretch region is not shown because of a very big solvent subtraction artifact.

solvent leaves the 2800-3100 cm^{-1} with large artifacts and this region is omitted from the spectra. The nominal C-I stretch fundamental and overtone bands have been shaded in Figs. 2-5.

The A-band resonance Raman spectra of iodoethane Figs. (2 and 5) have most of their intensity in the nominal C-I stretch overtone progression ($n\nu_{10}$).[89] The rest of the noticeable intensity appears in combination bands of the CCI bend, the CH_3 rock, the CH_2 wag, and the CH_3 antisymmetric stretch plus the nominal C-I stretch ($\nu_{11} + n\nu_{10}$, $\nu_8 + n\nu_{10}$, $\nu_7 + n\nu_{10}$, and $\nu_4 + n\nu_{10}$ respectively). The A-band resonance Raman spectra of 2-iodopropane (Fig. 3) also have most of their intensity in the nominal C-I stretch progression ($n\nu_8$). The rest of the significant intensity appears in combination bands of the CCI bend, the C-C stretch, CH_3 rock, and the HCC methine bend plus the nominal C-I stretch (ν_{10} +

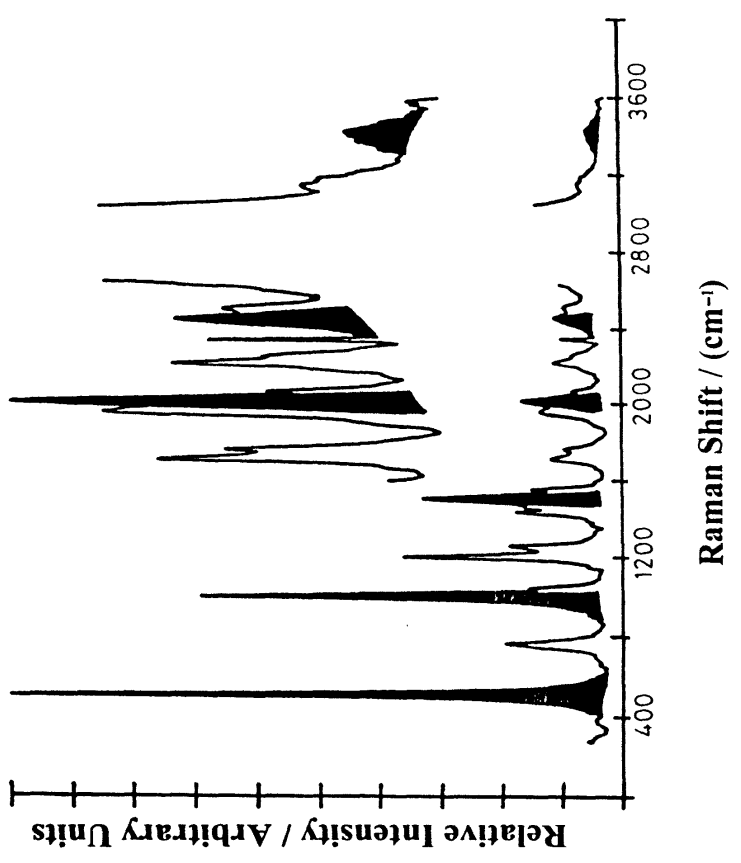

Fig. 5 Expanded view of the 258.2 nm iodoethane resonance Raman spectrum. The spectrum is intensity corrected and solvent subtracted. The shaded bands in the spectra are the nominal C-I stretch progression. The CH stretch region is not shown because of a very big solvent subtraction artifact.

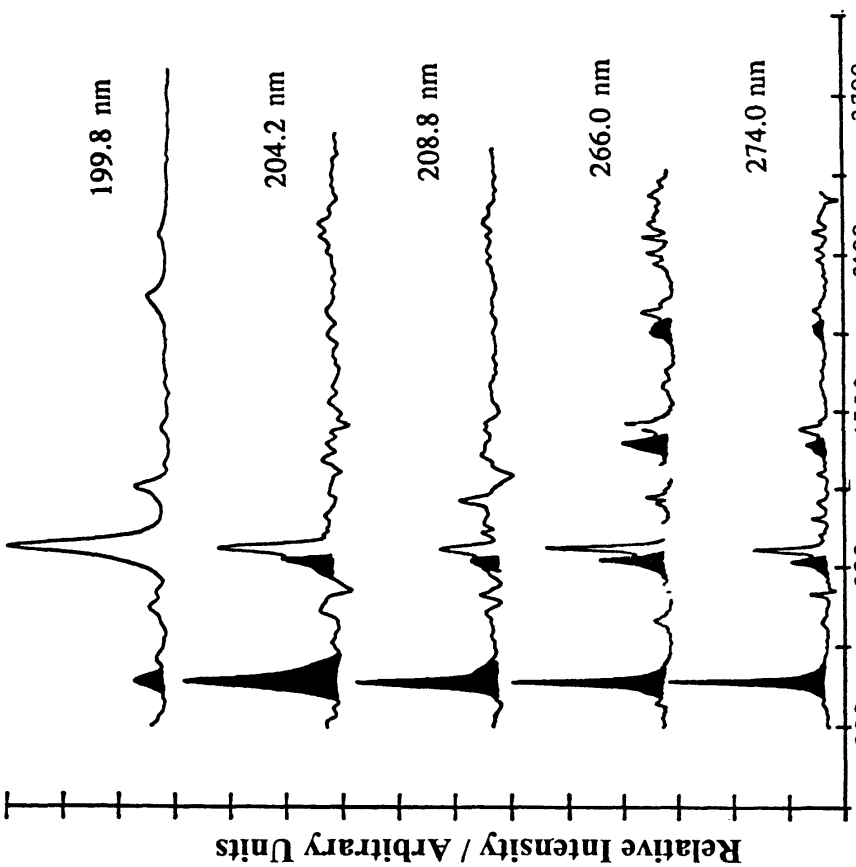

Fig. 6 Resonance Raman spectra of fully deuterated iodoethane in cyclohexane solution. The spectra have been intensity corrected and solvent subtracted. Small portions of of the 266.0 nm spectrum are not shown due to large solvent subtraction artifacts. The shaded bands in the spectra are the nominal C-I stretch progression.

nv_8, $v_7 + nv_8$, $v_5 + nv_8$, and $v_4 + nv_8$ respectively). The A-band resonance Raman spectra of 2-methyl-2-iodopropane have most of their intensity in the nominal C-I stretch progression (nv_7) and the combination band progression of the nominal CCI bend plus the C-I stretch ($v_8 + nv_7$). The remaining noticeable intensity appears in the combination bands of the C-C stretch and methyl rock plus the C-I stretch ($v_6 + nv_7$ and $v_5 + nv_7$ respectively). The resonance Raman spectra of iodoethane, 2-iodopropane, and 2-methyl-2-iodopropane display several common features and trends: the nominal C-I stretch progression has the largest amount of intensity in all the spectra, the second largest progression is the nominal CCI bend fundamental plus C-I stretch progression in all the spectra, and the intensity of the combination band progressions become larger as the molecule increases in size and/or becomes more branched relative to the C-I stretch overtone progression. In order to extract the A-band short-time photodissociation dynamics from the resonance Raman spectral intensities, there is a need to make a quantitative analysis using the normal mode descriptions for the Franck-Condon active modes.

Fig. 6 gives the resonance Raman spectra for the fully deuterated iodoethane isotopic derivative at five excitation wavelengths over the A-band and B-band region. The C-D stretch bands in the A-band region show no discernible intensity in combination bands or overtones and appear to arise mainly from presonance enhancement from the B-band or other higher energy states. This suggests that the C-H (D) stretches do not participate in the short-term photodissociation dynamics very much. The deuterated iodoethane resonance Raman spectra of Fig. 6 are noticeably different from the protonated spectra in Figs. 2 and 5. It is noted that the resonance Raman intensities in isotopically substituted molecules can be very useful in choosing among the many possible sign combinations of the excited-state displacement parameters.[2,5,8,89]

The depolarization ratios were measured for all three iodoalkanes with 266 nm excitation and the values for the C-I stretch fundamental obtained were 0.37, 0.39, and 0.34 (all ± 0.03) for iodoethane, 2-iodopropane and 2-methyl-2-iodopropane respectively.[89] These values are close to one third and suggest that most of the preresonant enhancement of the C-I stretch fundamental contributes to the same component of the Raman tensor as does the principal resonant contribution. The observed depolarization ratios of the first few overtones (~0.39) provides further support for this conclusion. The absolute resonance Raman cross sections for the nominal C-I stretch fundamental were measured for all of the Raman spectra shown in Figs. 2-6 and these values are listed in Table I. Inspection of Table I shows that the absolute cross sections preresonant to the B-band in the 200 to 230 nm region are much larger than those in the A-band region. Fig. 7 displays an A-term fit to the C-I stretch absolute Raman cross section preresonant to the B-band and an extrapolation of this fit into the A-band region. Fig. 7 clearly shows that the preresonant Raman contribution is of similar magnitude as the resonant contribution in the A-band and this is true for most of the iodoalkanes studied to date (including iodomethane). This gives rise to significant preresonant-resonant interference in the Raman excitation profile of the C-I stretch fundamental band in the A-band resonance Raman spectra. Since the preresonant contributions for combination bands and overtones decrease much faster than those for fundamentals as one goes farther from band responsible for the preresonant contribution, the preresonant-resonant interference

Table I

Measured nominal C-I stretch fundamental absolute resonance Raman cross sections at different wavelengths.

Absolute resonance Raman cross section (Å²/molecule)			
Wavelength (nm)	Iodoethane	2-Iodopropane	2-Methyl-2-Iodopropane
199.8	3.9×10^{-8}		
204.2	5.6×10^{-9}	1.4×10^{-8}	7.4×10^{-8}
208.8	3.0×10^{-9}	6.6×10^{-9}	3.3×10^{-8}
217.8	1.7×10^{-9}	3.6×10^{-9}	9.0×10^{-9}
223.1	8.7×10^{-10}	2.3×10^{-9}	3.8×10^{-9}
228.7			2.2×10^{-9}
258.2	5.0×10^{-11}		
266.0	2.0×10^{-10}	1.4×10^{-10}	8.3×10^{-11}
268.8			8.7×10^{-11}
270.3		1.9×10^{-10}	
274.0	2.4×10^{-10}		
276.6			1.3×10^{-10}
278.3		2.8×10^{-10}	
282.0	2.2×10^{-10}		
284.6			2.1×10^{-10}
302.6			1.7×10^{-10}

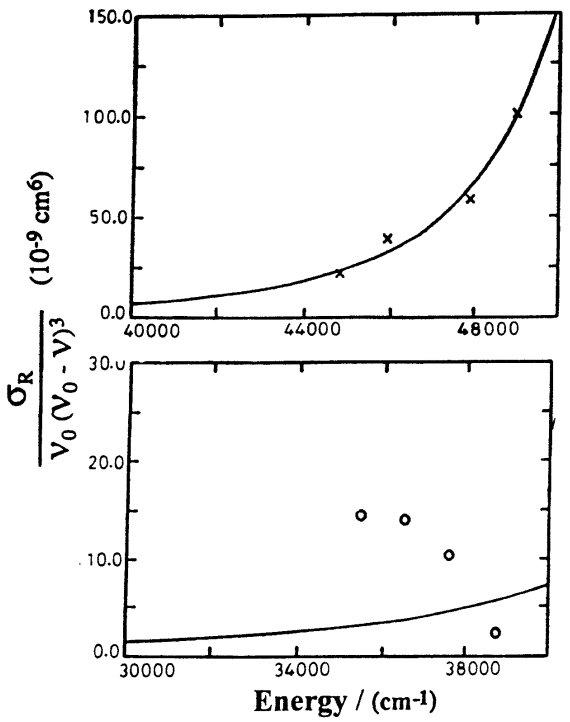

Fig. 7 The experimental absolute resonance Raman cross sections of the ν_{10} fundamental of iodoethane with excitation preresonant to the B-band absorption are shown by x in the top panel. The same measurements taken with A-band resonant wavelengths are given as o in the bottom panel. An Albrecht A-term fit is extrapolated into the A-band absorption region as presented in the bottom panel. The extrapolated preresonant contribution to the C-I stretch fundamental is not negligible compared with the experimental determinations of the C-I stretch fundamental cross sections in the A-band region.

is negligible for the overtones and combination bands of the A-band resonance Raman spectra. One can extract the short-time photodissociation dynamics from the A-band resonance Raman spectra by just modeling the overtones and combination band intensities. In order to simulate the fundamental Raman cross sections, one can use the A-term fits to the preresonant Raman cross sections to extrapolate into the A-band region and estimate the size of the preresonant contribution to the Raman tensor and calculate the fundamental cross sections. The equations and method of the fundamental calculations for the A-band iodoalkane resonance Raman intensities are given in detail in refs. [66] and [89]. The fundamental Raman bands of the A-band resonance Raman spectra of haloalkanes are susceptible to preresonant-resonant interference effects and care should be used in interpretation of their Raman intensities.[66,81,86,89]

The iodoethane, 2-iodopropane, and 2-methyl-2-iodopropane A-band absorption spectra and resonant absolute Raman cross sections were simulated using time-dependent wavepacket calculations as described in ref. [89] (for the overtones and combination bands these calculations are very similar to the description given in the Theory and Calculations section of this review article). The parameters for the best fit simulations are given in ref. [89] (also see ref. [69] for parameters for deuterated 2-iodopropane and 2-methyl-2-iodopropane). The spectra with excitation wavelengths nearer the A-band

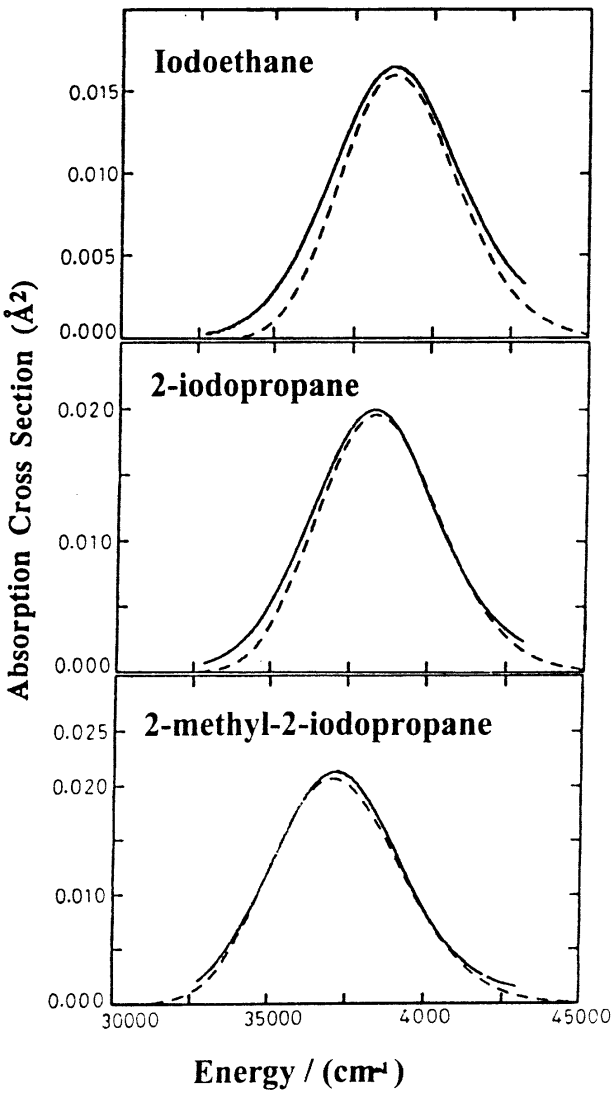

Fig. 8 Comparison of the A-band experimental (solid lines) and calculated (dashed line) absorption spectra. The dashed curves are calculated using the best fit parameters and model given in reference [89].

maximum were given greater weight in determining the best fit simulation parameters since the dominant $^3Q_0$ transition makes its largest contribution near the center of the absorption band. Fig. 8 presents a comparison of the calculated and experimental A-band absorption spectra for iodoethane, 2-iodopropane, and 2-methyl-2-iodopropane. There is reasonable agreement between the calculated and experimental absorption spectra in Fig. 8 taking into account we

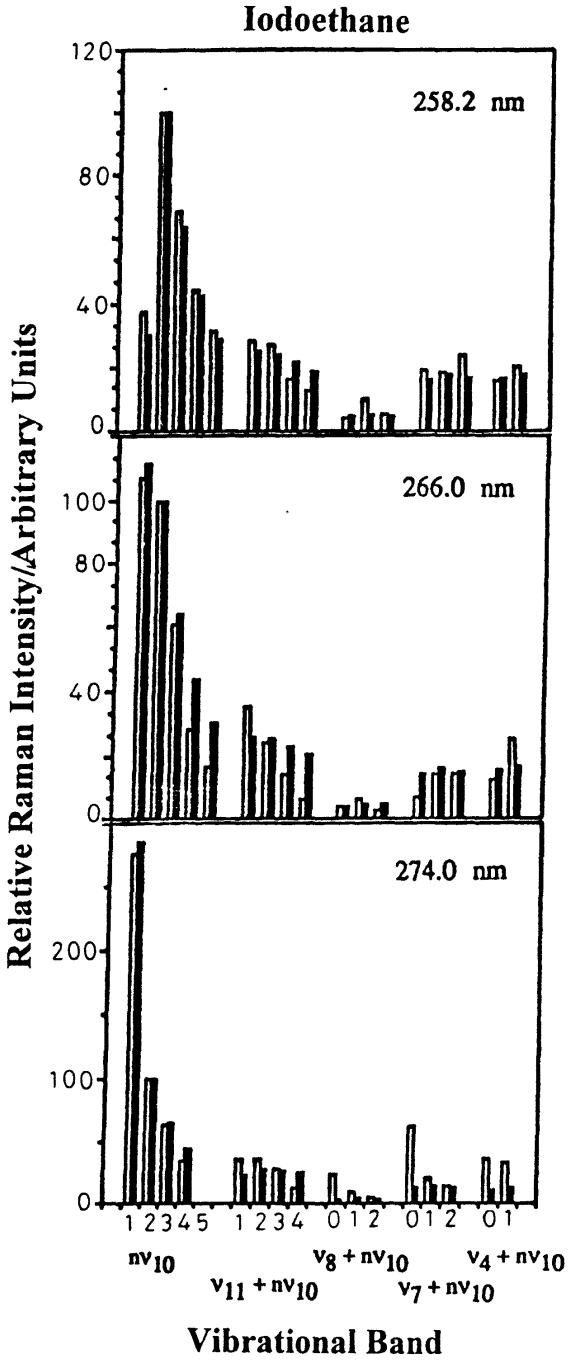

Fig. 9 Comparison of the experimental (open bars) and calculated (solid bars) relative Raman intensities for three A-band excitation wavelengths for iodoethane. The best fit parameters and model given in reference [89] were used for the calculations.

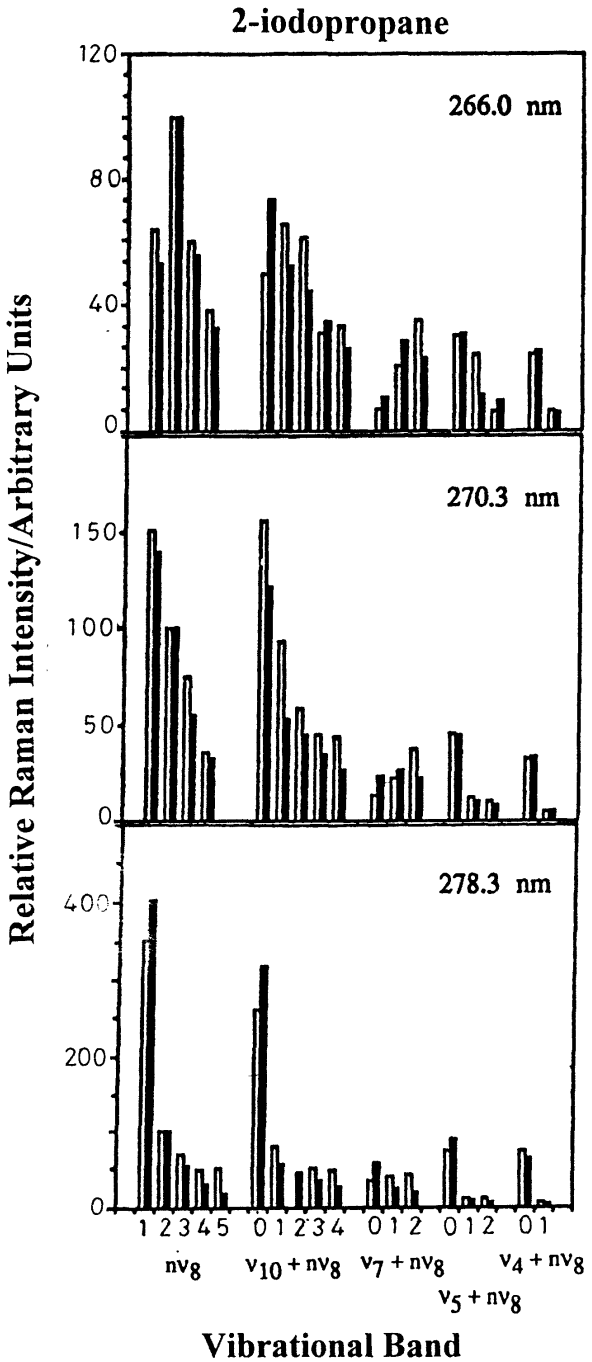

Fig. 10 Comparison of the experimental (open bars) and calculated (solid bars) relative Raman intensities for three A-band excitation wavelengths for 2-iodopropane. The best fit parameters and model given in reference [89] were used for the calculations.

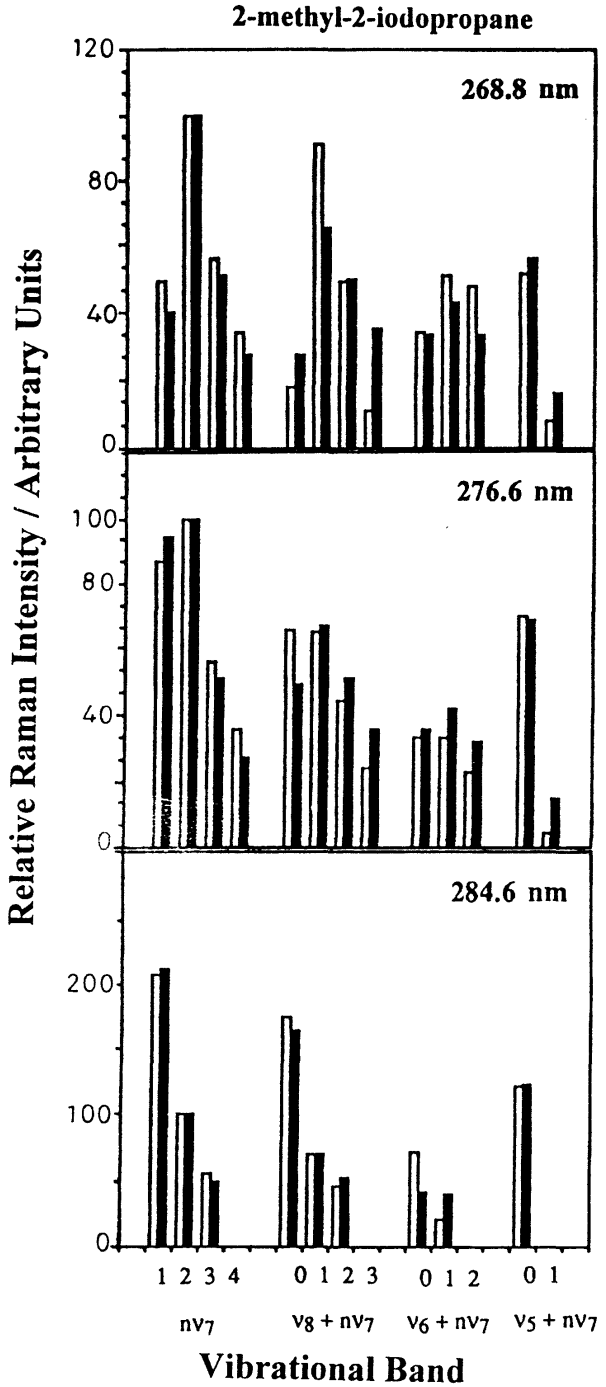

Fig. 11 Comparison of the experimental (open bars) and calculated (solid bars) relative Raman intensities for three A-band excitation wavelengths for 2-methyl-2-iodopropane. The best fit parameters and model given in reference [89] were used for the calculations.

are neglecting the small contributions of the $^3Q_1$ and $^1Q_1$ to the red and blue edges of the A-band absorption. Figs. 9-11 display comparisons of the calculated and experimental A-band resonance Raman intensities for iodoethane, 2-iodopropane, and 2-methyl-2-iodopropane in cyclohexane solution. There is generally good agreement between the experimental and calculated Raman intensities and provides confidence that the simulation parameters can be used to extract the major features of the short-time photodissociation dynamics.

Fig. 12 presents the experimental ratio of the fundamental to the first overtone ($\nu_{10}/2\nu_{10}$) for the nominal C-I stretch for iodoethane compared to the same ratio obtained from simulations including the preresonant contributions from higher energy excited states and simulations which do not include preresonant contributions. Good agreement between the experimental values and the simulations occurs when one includes the preresonant contribution. Fig. 12 illustrates the importance of preresonant-resonant interferene in simulating the observed fundamental intensities in iodoalkanes.[66,81,85,89]

Using the results of normal coordinate calculations for iodoethane, 2-iodopropane, and 2-methyl-2iodopropane (described in reference and its supplementary material) and eqs. (3) and (4) we can obtain the possible range of internal coordinate displacements associated with the short-time photodissociation dynamics. Because the simulation parameters of refs. [89] and [69] only give the absolute magnitude of each normal mode displacement, 2^n different choices for the n Franck-Condon active normal modes are consistent with the simulation results.[2,5,8,89] We can eliminate half of these possible sign combinations by making use our chemical knowledge about direct photodissociation reactions: direct cleavage of the C-I bond should lengthen the C-I bond. We can further reduce the number of possible sign combinations by using the redundancy present in the resonance Raman intensities of isotopic derivatives. Since the electronic structure is invariant with isotopic substitution, the isotopic derivatives should all have the same photodissociation dynamics but they usually have different resonance Raman intensities. Each possible choice of sign for each isotopic derivative will give a different excited state geometry and the geometry that has the least variance across a set of isotopic derivatives is chosen as the most possible short-time photodissociation dynamics. The reader is referred to an excellent review article by Myers[5] for further discussion of the problem of choosing

Table II

Most Probable Internal Coordinate Displacements at t=10 fs After Photoexcitation for Iodoethane, 2-Iodopropane, and 2-Methyl-2-Iodopropane.

Compound	Coordinate	Range of Displacements at 10 fs
Iodoethane[a]	r_{C-I}	+0.13 to +0.15 Å
	r_{BC}	–0.06 to –0.05 Å
	∠BCI	–6° to –3°
	∠HCI	–7° to –3°
	$\angle BCH_6$	+6° to +9°
	$\angle H_6CH_7$	–6° to +5°
	$\angle CBH_2$	–1° to +5°
	$\angle CBH_3$	–1° to –3°
	$\angle H_2BH_3$	–4° to +5°
	$\angle H_2BH_4$	–8° to +8°
2-Iodopropane[b]	r_{C-I}	+0.09 to +0.12 Å, [c]
	r_{BC}	+0.02 to +0.05 Å, [c]
	∠BCI	–2.7° to –4.2°, [c]
	∠BCB	–2° to +5°
	$\angle H_7CI$	–3° to +5°
	$\angle BCH_7$	–1° to +6°
	$\angle CBH_2$	–10° to +4°
	$\angle CBH_3$	–10° to +5°
	$\angle CBH_4$	–1° to +8°
	$\angle H_2BH_3$	–3.6° to +1.3°, [c]
	$\angle H_2BH_4$	–1° to –2°, [c]
	$\angle H_3BH_4$	–2° to +2°, [c]
2-Methyl-2-Iodopropane[d]	r_{C-I}	+0.03 to +0.12 Å, [e]
	r_{BC}	+0.03 to +0.05 Å, [e]
	∠BCI	–2° to –4.7°, [e]
	∠BCB	+1° to +6°
	$\angle CBH_4$	–4° to +7°
	$\angle H_4BH_5$	–3.5° to +1°, [e]
	$\angle H_4BH_6$, $\angle H_5BH_6$	–1.6° to –0.9°, [e]

[a] Values from ref. [89] and comparison of fully protonated and deuterated iodoethane data.
[b] Values from ref. [89].
[c] Values have been narrowed by using comparison with a deuterated isotopic derivative set data (see ref. [69]).
[d] Values from ref. [89].
[e] Values from reference have been narrowed by using comparison with a deuterated isotopic derivative set of data (see ref. [69]).

the sign of the normal mode displacements. In ref. [89] we made comparisons of fully protonated and deuterated derivatives of iodoethane to help eliminate most of the possible sign combinations of the normal mode displacement parameters. Further comparisons to deuterated derivatives of 2-iodopropane and 2-methyl-2-iodoproane were done to help narrow the possible number of sign combinations (see ref. [69]). Table II lists the most probable A-band short time photodissociation dynamics at 10 fs derived from resonance Raman intensity analysis of iodoethane, 2-iodopropane, and 2-methyl-2-iodopropane by author's group.

Inspection of Table II shows that the C-I bond cleavage short-time dynamics are multidimensional in nature with significant motion along other parts of the molecule other than the C-I bond alone. The C-I bond lengthens faster in iodoethane than in the larger iodoalkanes (+0.13 to +0.15 Å for iodoethane, +0.09 to +0.12 Å for 2-iodopropane and +0.03 to +0.12 Å for 2-methyl-2-iodopropane) and these results display a good correlation with the amount of internal energy found in the radical photoproducts and the widths of their internal energy distributions measured in previous time-of-flight photofragment spectroscopy experiments (for example, the internal excitation of the alkyl radical increases from 28% to 38% for iodoethane[19,20,24,52] to 43% to 67% in 2-iodopropane[19,20,25]). Both the short-time and long time dynamics suggest that less of the absorption photon energy goes into cleaving the C-I bond with more energy partitioned to changing the structure of the rest of the molecule in 2-iodopropane than in iodoethane. Our results in Table II also suggest that the larger amount of energy partitioned to the alkyl group as the alkyl group becomes more massive and/or branched starts in the Franck-Condon region of the photodissociation reaction. This implies that the $^3Q_0$ to $^1Q_1$ curve crossing probability is affected by this Franck-Condon region energy partitioning in addition to mass effects. The C-C bond(s) shorten in iodoethane but lengthen in 2-iodoproane and 2-methyl-2-iodopropane. The parent iodoalkanes have C-C bond lengths of 1.54 Å in their ground electronic states and the corresponding alkyl radicals have C-C bond lengths ~1.49 Å in their ground electronic states as determined in several *ab initio* investigations.[91-93] The initial short-time dynamics of C-I bond cleavage in iodoethane brings the ethyl group C-C bond length closer toward the value found for the ground state ethyl radical. However, the initial photodissociation motion is in the opposite direction for 2-iodopropane and 2-methyl-2-iodopropane. This would suggest that there will be less C-C vibrational excitation of the nascent ethyl radical

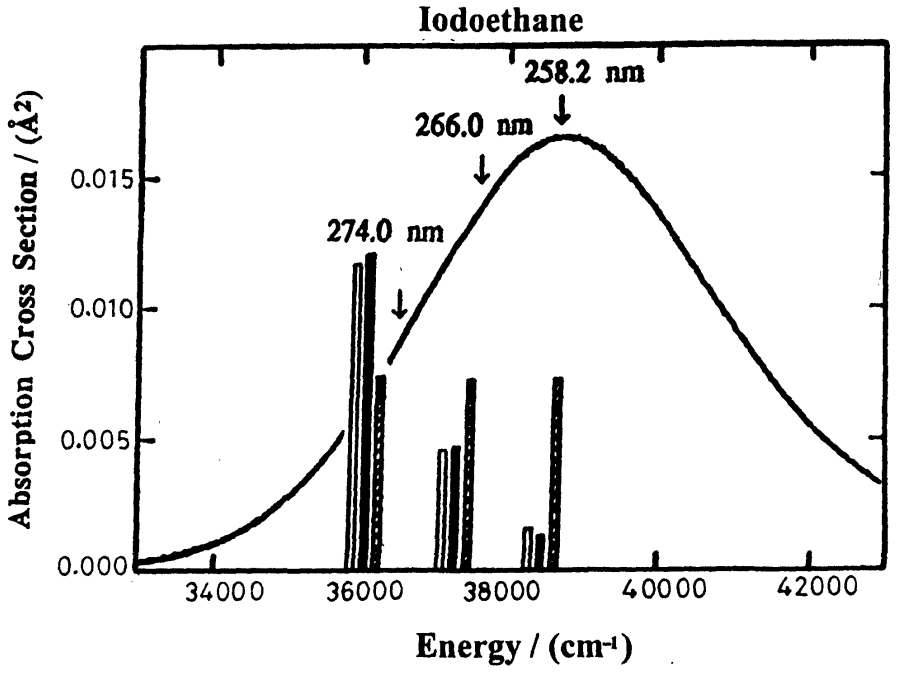

Fig. 12 Experimental ratio of the nominal C-I stretch fundamental to its first overtone ($\nu_{10}/2\nu_{10}$) for iodoethane in cyclohexane solution (open bars) compared to the same ratio calculated including the nonresonant A-term contributions (solid bars) and the ratio calculated without the nonresonant contribution (striped bars). The A-band absorption spectrum for iodoethane is shown for reference.

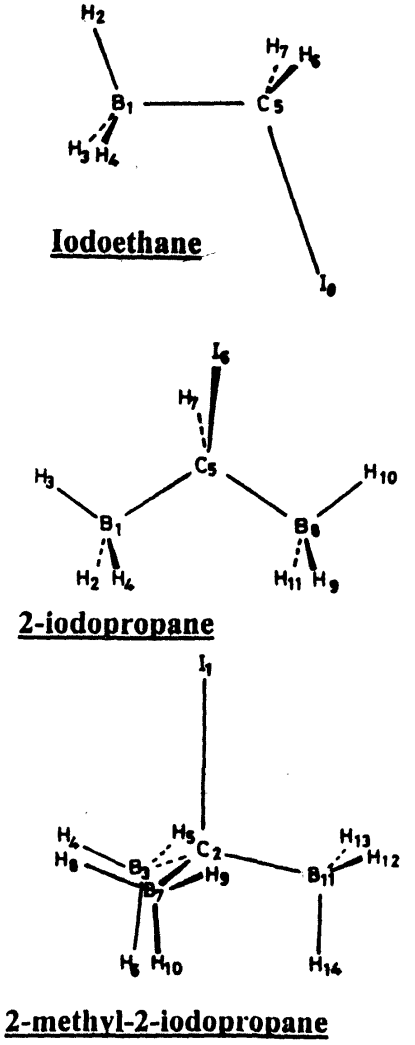

Fig. 13 Simple diagrams of the geometries of iodoethane (top), 2-iodopropane (middle), and 2-methyl-2-iodopropane (bottom). The CH bond length is 1.09 Å, the CC bond length is 1.54 Å, the CI bond length is 2.135 Å, and the angles are 109.5 degrees (e.g. a tetrahedral geometry about the carbon atoms). C represents the α-carbon atoms, B represents the β-carbon atoms, H are hydrogen atoms, and I are iodine atoms.

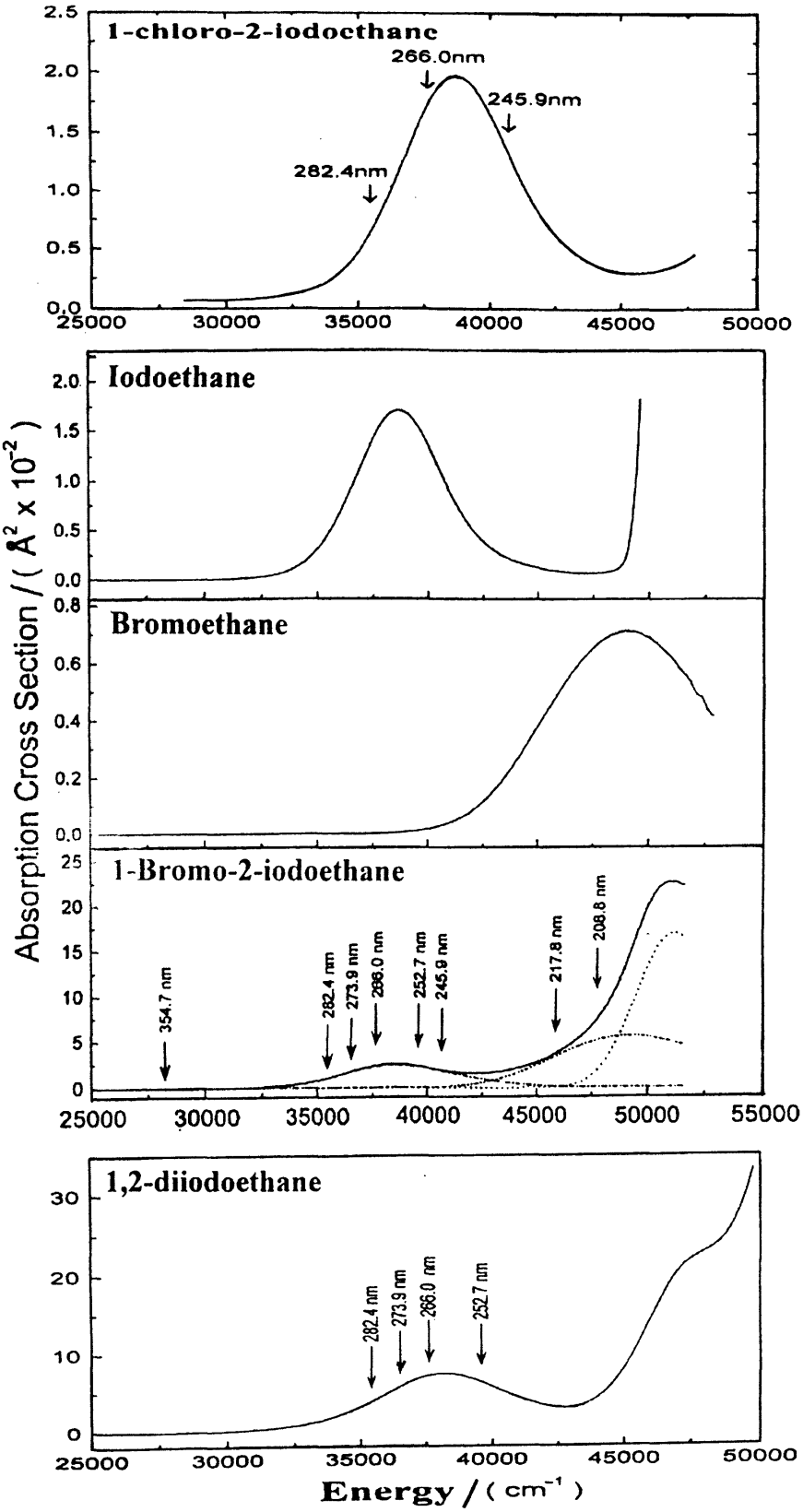

Fig. 28 Absorption spectra of 1-chloro-2-iodoethane, iodoethane, bromoethane, 1-bromo-2-iodoethane, and 1,2-diiodoethane in cyclohexane solution. The excitation frequencies for the resonance Raman spectra are shown above the 1-chloro-2-iodoethane, 1-bromo-2-iodoethane, and 1,2-diiodoethane spectra.

dynamics of both the A-band and B-band are consistent with an impulsive "semi-rigid" radical description of the photodissociation with the CH_2Br radical group moving towards a more planar structure in the A-band and the CH_2I radical group moving towards a more planar structure in the B-band. We have done a gaussian deconvolution of the A-band and B-band absorption spectra of bromoiodomethane in order to estimate the relative contributions of the different $n \rightarrow \sigma^*$ transitions to the absorption bands. The comparison of this gaussian deconvolution for bromoiodomethane with the deconvolutions for the corresponding single chromophore molecules (e.g. bromomethane and iodomethane) indicates that the $^3Q_0$ transition receives significantly more enhancement of its oscillator strength than the $^1Q_1$ and $^3Q_1$ transitions as one goes from the single chromophore molecule to the two chromophore bromoiodomethane molecule. In addition, the B-band transitions have their oscillator strengths enhanced to a noticeably greater extent than the A-band transitions in bromoiodomethane. The patterns in the gaussian deconvolutions of the absorption spectra, the experimental resonance Raman intensities and the deduced short-time photodissociation dynamics of bromoiodomethane all suggest a noticeable amount of coupling between the C-I and C-Br chromophores. The reader is referred to ref. [67] for more details on this prototypical molecule for bond selective electronic excitation and photochemistry as well as a hypothesis for the B-band photodissociation reactions that is consistent with our results and those of previous molecular beam experiments.[96-98]

E. Substituent Effects and Influence of a Second Carbon-Halogen Chromophore in 1-Halo-2-Iodoethanes

We have investigated the A-band photodissociation dynamics of three dihaloethanes (1-chloro-2-iodoethane, 1-bromo-2-iodoethane, and 1,2-diiodoethane) in order to examine substituent effects on the photodissociation dynamics and how the presence of an additional carbon-halogen

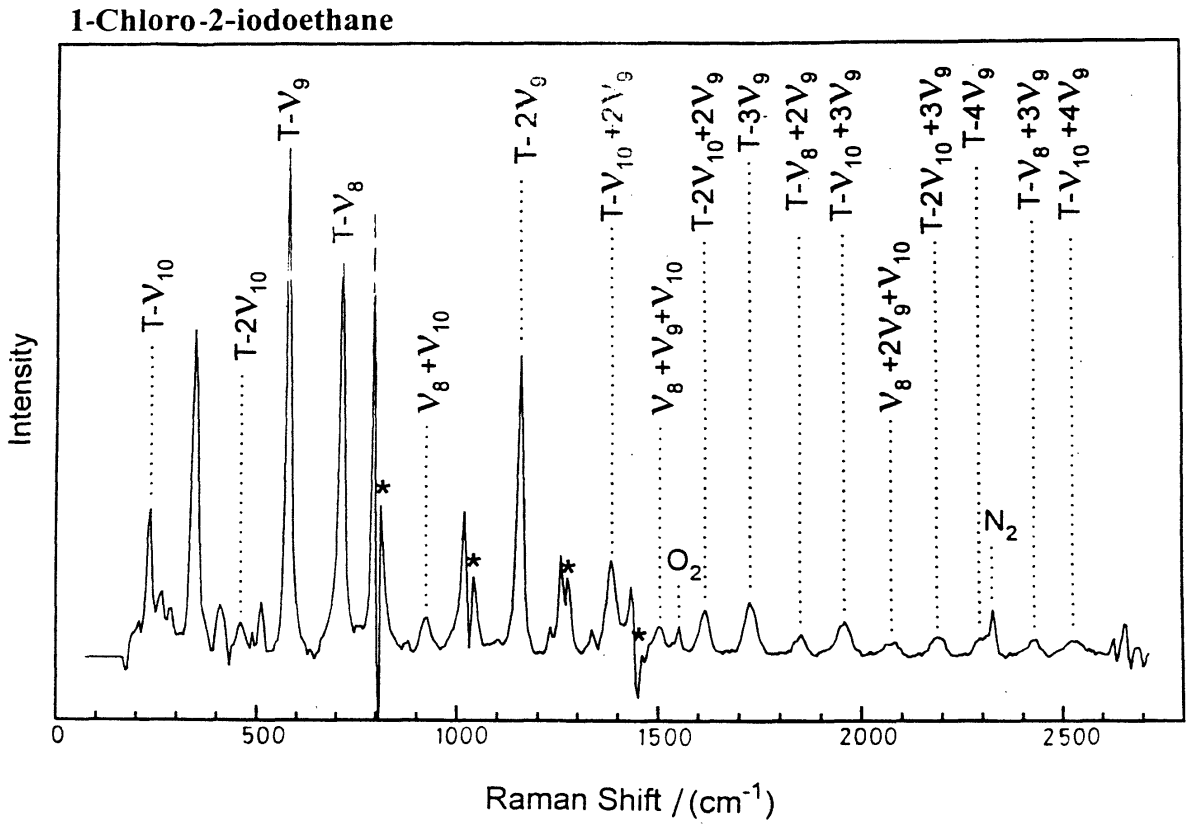

Fig. 29 Enlarged view of the 266.0 resonance Raman spectrum of 1-chloro-2-iodoethane in cyclohexane solution. The spectrum has been intensity corrected and solvent subtracted. Regions with solvent subtraction artifacts have been marked by asterisks. The more intense Raman bands have their tentative assignments displayed.

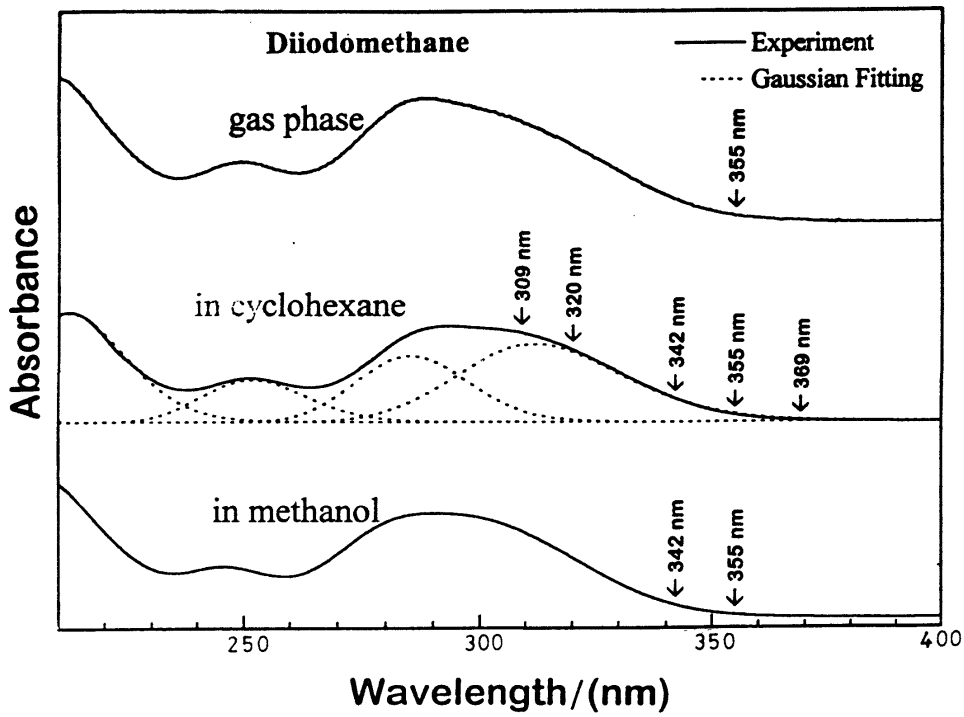

Fig. 17 Diiodomethane absorption spectra in the gas phase, in cyclohexane solution and in methanol solution. The resonance Raman excitation wavelengths are indicated by the arrows and numbers (in nm) above each spectrum. The dashed lines represent a best fit Gaussian deconvolution of the absorption spectrum.

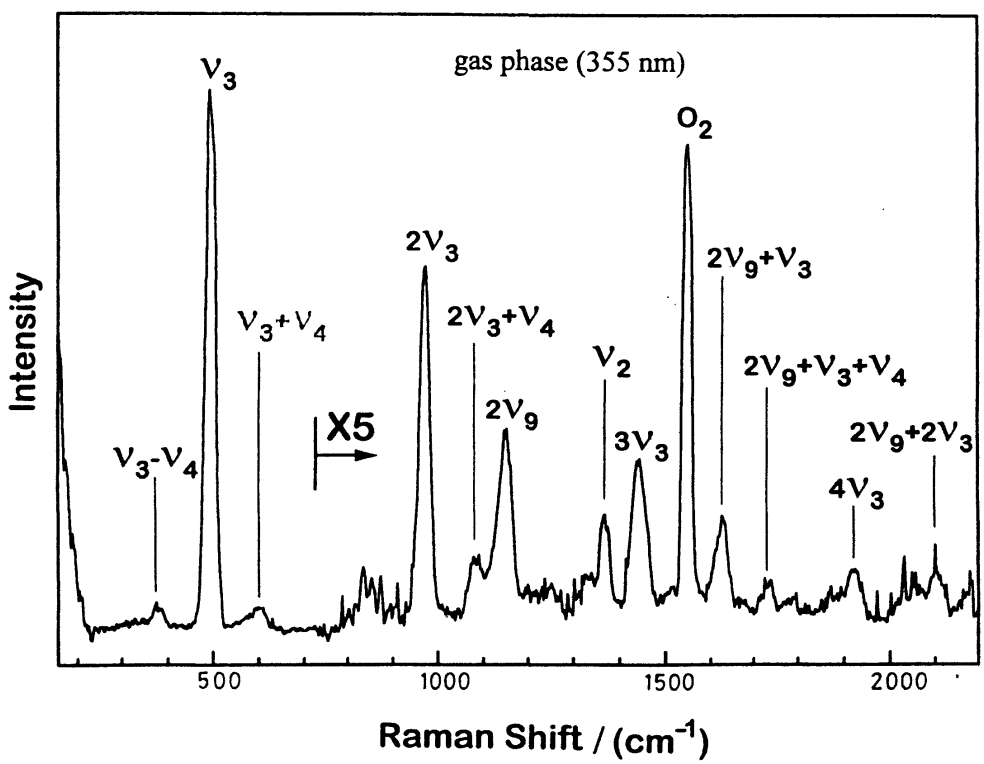

Fig. 18 Gas phase diiodomethane 355 nm resonance Raman spectrum. The spectrum has been intensity corrected and the assignments of the larger Raman bands are given.

Table III

(A.) Parameters for calculation of resonance Raman intensities and absorption spectrum of vapour phase diodomethane and diiodomethane in methanol solution. (B.) Most probable internal coordinate displacements of diiodomethane at t= 15 fs assuming the C-I bond becomes longer.

(A.) Vapour Phase Diiodomethane	Transition length, M=0.197 Å, E_0 = 25,700 cm^{-1}		
Vibrational Mode	Ground state Vibrational Frequency (cm-1)	Excited state Vibrational Frequency (cm-1)	|Δ|
ν_4 (I-C-I bend)	134 cm^{-1}	134 cm^{-1}	5.6
ν_3 (I-C-I symmetric stretch)	499 cm^{-1}	499 cm^{-1}	4.0
ν_9 (I-C-I anti-symmetric stretch)	581 cm^{-1}	-770 cm^{-1}	0.00
ν_2 (CH_2 scissor)	1379 cm^{-1}	1379 cm^{-1}	0.56
Diiodomethane in Methanol Solution	Transition length, M=0.256 Å,	E_0 = 25,800 cm^{-1}	
Vibrational Mode	Ground state Vibrational Frequency (cm^{-1})	Excited state Vibrational Frequency (cm^{-1})	|Δ|
ν_4 (I-C-I bend)	141 cm^{-1}	180 cm^{-1}	5.9
ν_3 (I-C-I symmetric stretch)	501 cm^{-1}	501 cm^{-1}	2.4
ν_9 (I-C-I anti-symmetric stretch)	585 cm^{-1}	780 cm^{-1}	1.3
ν_5 (CH_2 twist)	1032 cm^{-1}	1032 cm^{-1}	0.24
ν_2 (CH_2 scissor)	1375 cm^{-1}	1375 cm^{-1}	0.24

(B.) Short-Time Photodissociation Dynamics at t=15 fs After Photoexcitation

Internal Coordinate	Gas Phase [a]15 fs	Solution Phase (in methanol solvent) [b]15 fs with Δ_9=+1.3	[c]15 fs with Δ_9=-1.3
C-H bonds	-0.008 Å (-0.009 Å)	-0.004 Å (-0.006 Å)	-0.004 Å (-0.006 Å)
C-I bond, atoms 1 and 4	+0.146 Å (+0.142 Å)	+0.169 Å (+0.162 Å)	+0.010 Å (+0.004 Å)
C-I bond, atoms 1 and 5	+0.146 Å (+0.142 Å)	+0.010 Å (+0.004 Å)	+0.169 Å (+0.162 Å)
H-C-H angle, atoms 2, 1, and 3	-2.4° (-2.5°)	-1.5° (-1.4°)	-1.5° (-1.4°)
H-C-I angle, atoms 2, 1, and 4	+2.8° (+3.2°)	-0.4° (+0.1°)	+3.5° (+4.0°)
H-C-I angle, atoms 3, 1, and 5	+2.8° (+3.2°)	+3.5° (+4.0°)	-0.4° (+0.1°)
H-C-I angle, atoms 2, 1, and 5	+2.9° (+3.3°)	+3.5° (+4.0°)	-0.2° (+0.3°)
H-C-I angle, atoms 3, 1, and 4	+2.9° (+3.3°)	-0.2° (+0.3°)	+3.5° (+4.0°)
I-C-I angle, atoms 4, 1, and 5	-8.9° (-11°)	-4.9° (-7.0°)	-4.9° (-7.0°)

[a]Values without parentheses are for the sign combination of Δ_3=-4.0 and Δ_4=+5.6, while values within parentheses are for the sign combination of Δ_3=-4.0 and Δ_4=-5.6.

[b]Values without parentheses are for the sign combination of Δ_3=-2.4, Δ_4=+5.9, and Δ_9=+1.3 while values within parentheses are for the sign combination of Δ_3=-2.4 and Δ_4=-5.9, and Δ_9=+1.3.

[c]Values without parentheses are for the sign combination of Δ_3=-4.0, Δ_4=+5.9, and Δ_9=-1.3 while values within parentheses are for the sign combination of Δ_3=-4.0 and Δ_4=+5.9, and Δ_9=-1.3.

cyclohexane solution (369 nm, 355 nm, and 342 nm).[62,65] The resonance Raman spectra have most of their intensity in the fundamentals, overtones, and combination bands associated with the nominal I-C-I symmetric stretch, I-C-I bend, and I-C-I anti-symmetric stretch vibrational modes. The A-state absorption spectra and resonance Raman intensities were simulated using time-dependent wavepacket

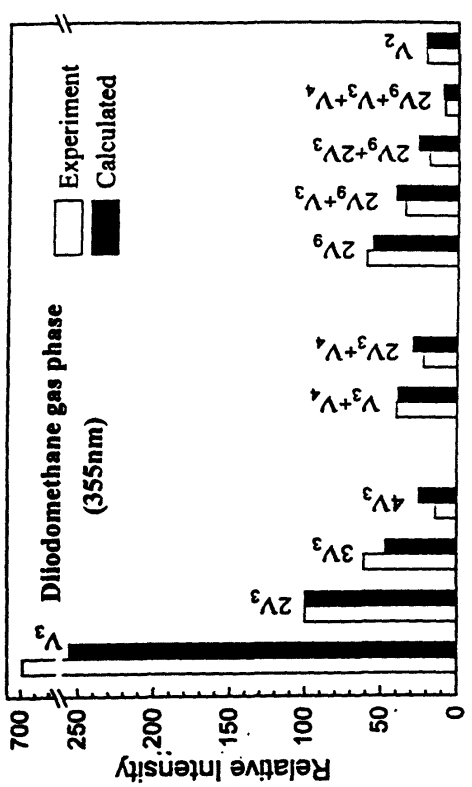

Fig. 20 Comparison of experimental (open bars) and calculated (solid bars) resonance Raman intensities for the gas phase diiodomethane 355 nm resonance Raman spectrum. Comparison of the experimental (solid line), Gaussian band of the A-state deconvolution (dashed line), and calculated (dotted line) absorption spectra. The calculations made use of the parameters and simple model given in reference [65].

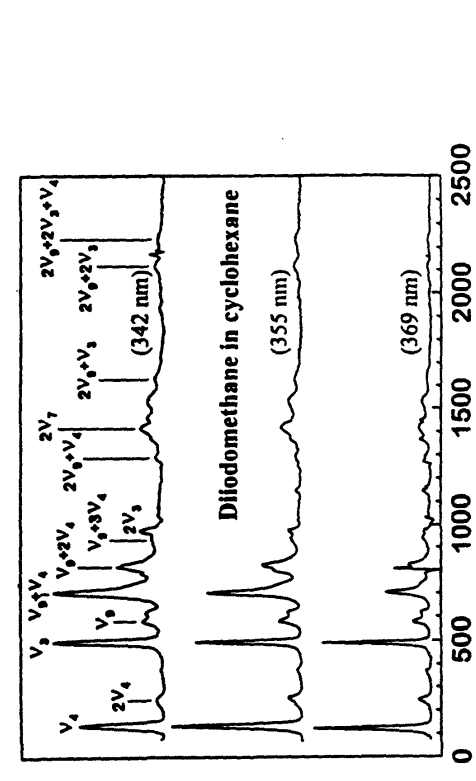

Fig. 19 Resonance Raman spectra of solution phase diiodomethane in cyclohexane and methanol solvents. The spectra have been intensity corrected and solvent subtracted. The asterisks mark portions of the spectra with solvent subtraction artifacts. The assignments of the larger Raman bands are also shown.

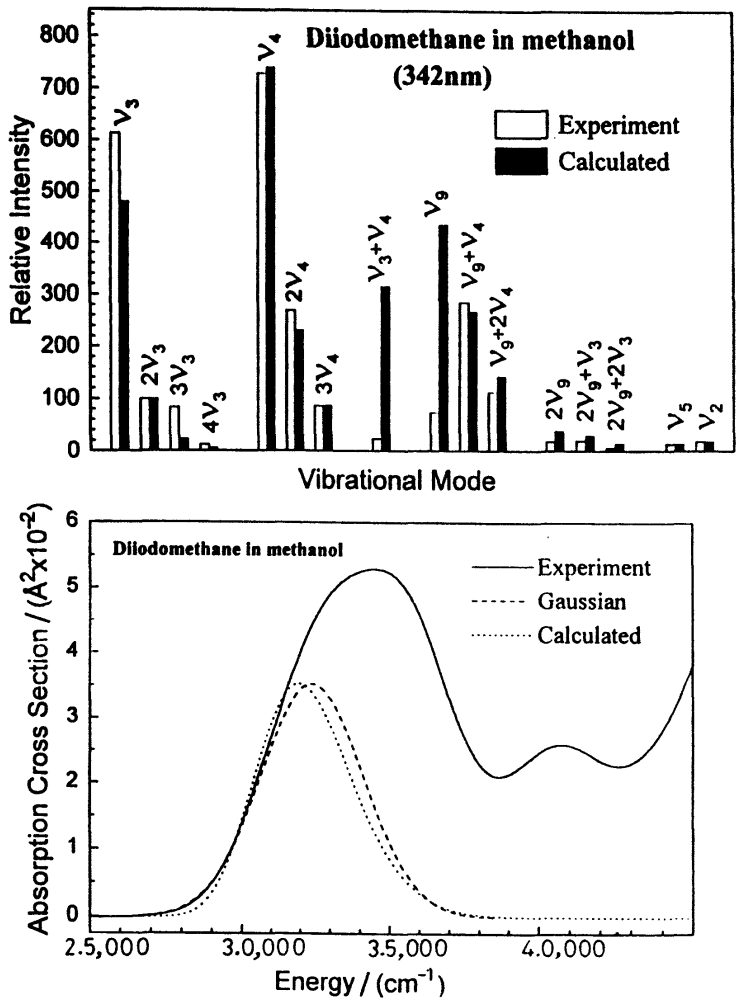

Fig. 21 Comparison of experimental (open bars) and calculated (solid bars) resonance Raman intensities for the solution phase diiodomethane in methanol solvent 342 nm resonance Raman spectrum. Comparison of the experimental (solid line), Gaussian band of the A-state deconvolution (dashed line), and calculated (dotted line) absorption spectra. The calculations made use of the parameters and simple model given in reference [65].

calculations and a simple model similar to that described in the Theory and Calculations section (also described in detail in ref. [65]). Comparisons of the experimental and the best fit calculated absorption spectra and the resonance Raman intensities are shown in Fig. 20 for the gas phase and Fig. 21 for the methanol solution. Considering the simple model we used in the simulations, we obtain reasonable agreement between the calculated and experimental data. The best fit simulation parameters are listed in Table III. The normal mode coefficients from normal coordinate calculations (described in ref. [65] and its supplementary material) were used in conjunction with eqs. (3) and (4) to convert the motion of the wavepacket on the excited state from

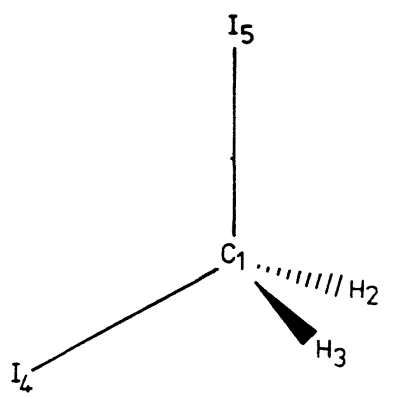

Fig. 22 Geometry of diiodomethane with each atom labeled with a number 1 through 5. All C-H bond lengths are 1.093 Å, the C-I bond lengths are 2.1195 Å, and all bond angles are 109.45°.

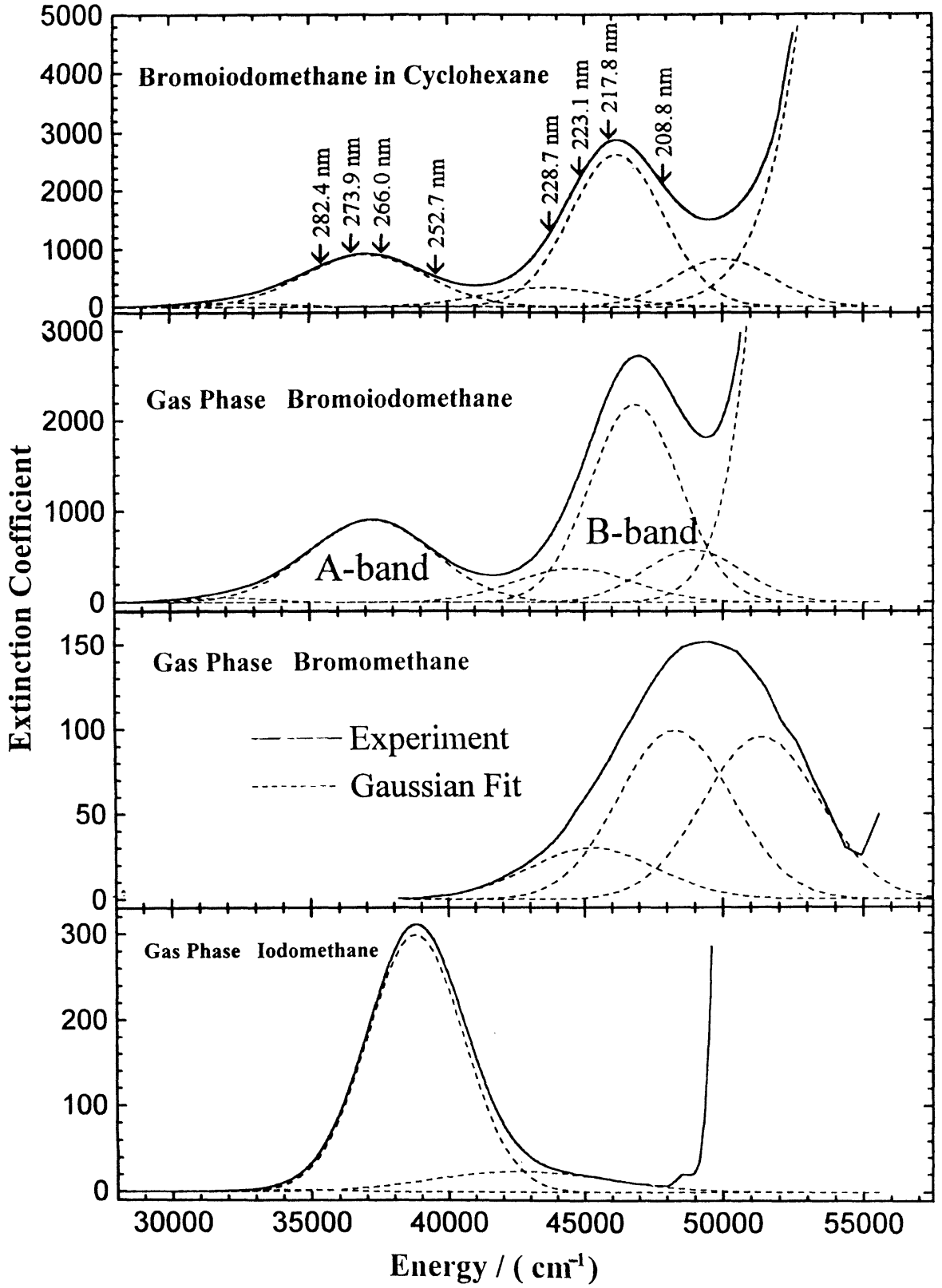

Fig. 23 Absorption spectra of bromoiodomethane in cyclohexane solution and in the gas phase. Absorption spectra for gas phase bromomethane and iodomethane are also displayed. Gaussian curve fits to the absorption spectra are given by dashed lines. The resonance Raman excitation frequencies for the bromoiodomethane in cyclohexane solution experiments are shown above its absorption spectrum.

dimensionless normal coordinates into internal coordinates of the molecule. It is assumed that the C-I bond becomes longer in the excited state because the A-state photodissociates in a direct manner. Table III presents the short time photodissociation dynamics obtained for t=15 fs after photoexcitation for diiodomethane in the gas phase and in methanol solution and the simple diagram of the diiodomethane molecule in Fig. 22 can be used to better visualize the dynamics

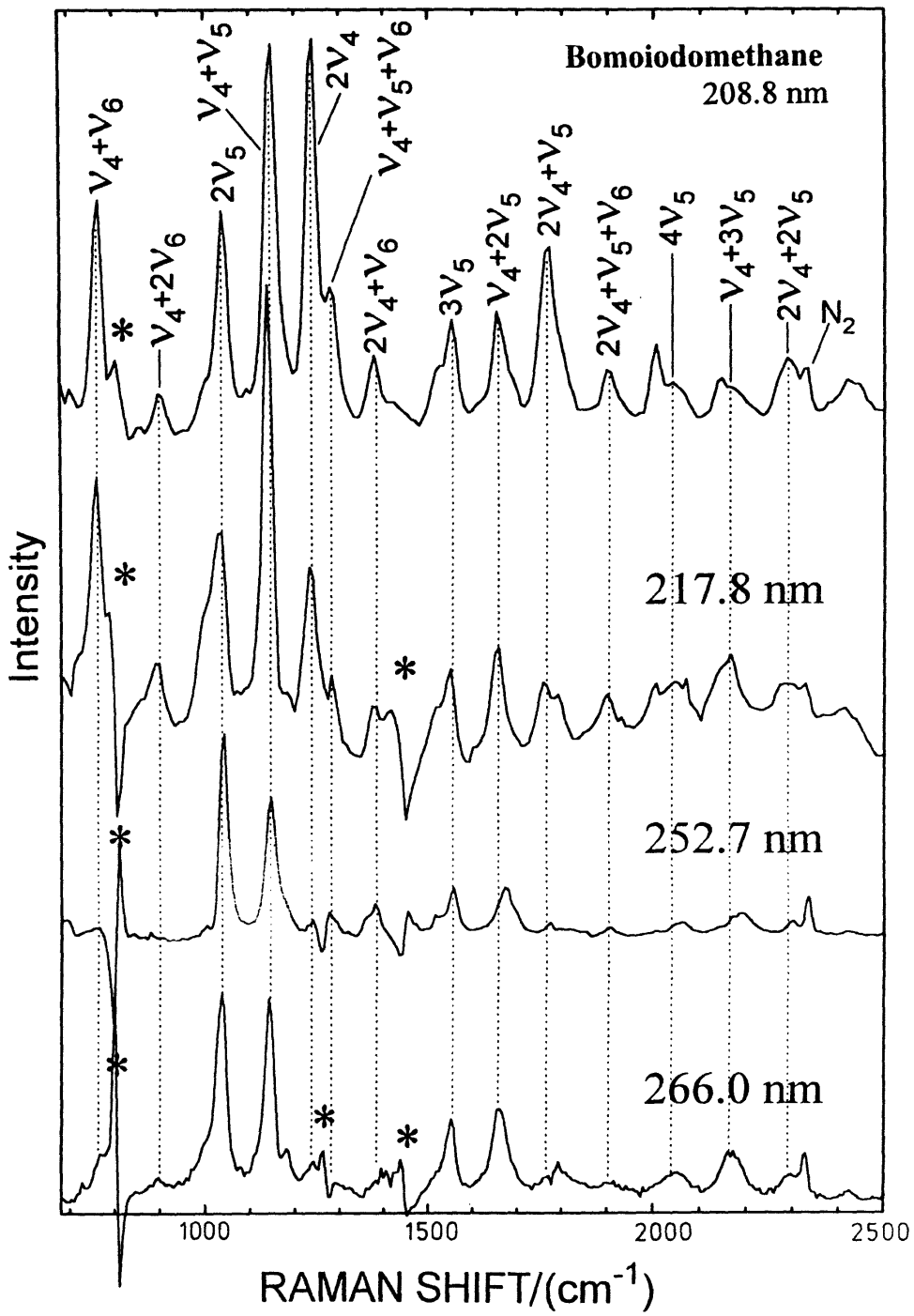

Fig. 24 Enlarged views of the B-band 208.8 and 217.8 nm resonance Raman spectra and the A-band 252.7 and 266.0 nm resonance Raman spectra. The spectra have been intensity corrected and solvent subtracted (asterisks indicate regions with solvent subtraction artifacts). The tentative assignments of some of the larger Raman bands are shown above the spectra.

presented in Table III. Inspection of Table III shows that the two C-I bonds lengthen by the same amount, the I-C-I becomes smaller, the H-C-I becomes larger, and the H-C-H angle becomes smaller in the A-state gas phase short-time photodissociation dynamics. The two C-I bonds appear equivalent in the Franck-Condon region of the gas phase photodissociation and this indicates that the molecule decides which of the two bonds are broken after the wavepacket has left the Franck-Condon region of the surface. The lack of intensity in the I-C-I anti-symmetric stretch fundamental and odd overtones or combination bands of the fundamental with other modes in the gas phase resonance Raman spectrum (see Fig. 18) is due to this symmetry of the two C-I bonds in the gas phase Franck-Condon region of the dissociation. Comparison of the gas and solution phase resonance Raman spectra indicates that there is a large solvent-induced symmetry breaking. This gives rise to significant intensity in the I-C-I anti-symmetric stretch fundamental and odd overtones or combination bands of the fundamental with other modes in the solution phase resonance

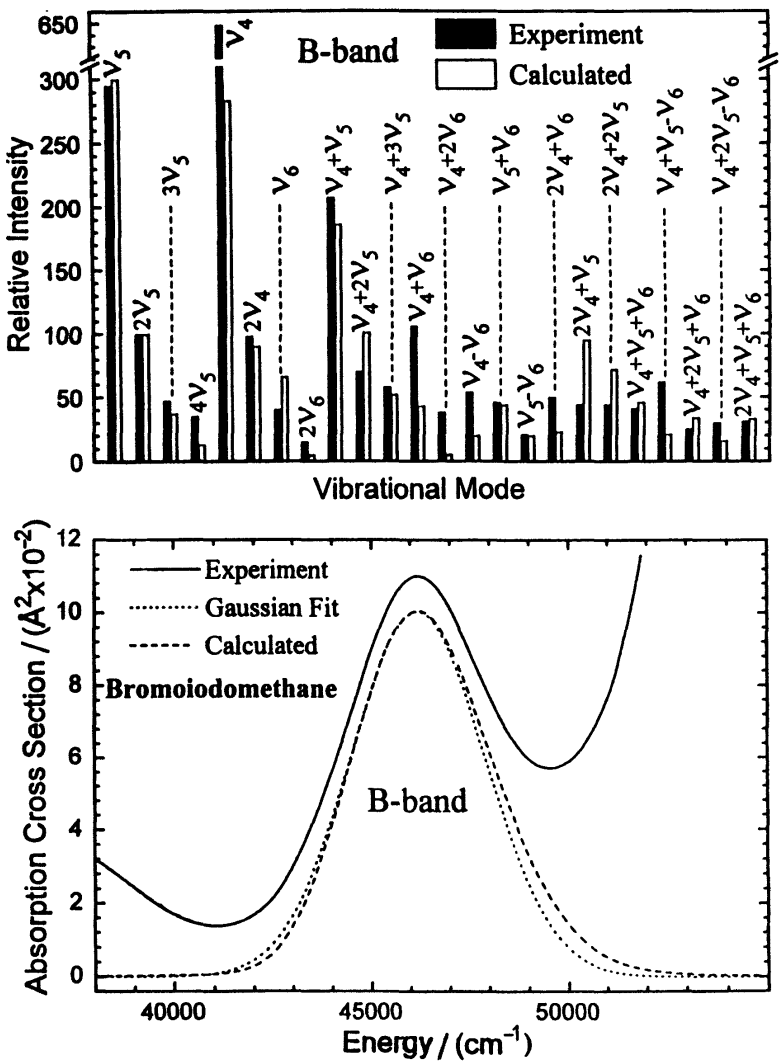

Fig. 25 Comparison of experimental (solid bars) and calculated (open bars) resonance Raman intensities for the solution phase bromoiodomethane in cyclohexane solvent 217.8 nm resonance Raman spectrum. Comparison of the experimental (solid line), Gaussian band of the A-state deconvolution (dotted line), and calculated (dashed line) B-band absorption spectra for bromoiodomethane in cyclohexane solution. The calculations made use of the parameters and simple model given in reference [67].

Raman spectra that are not observed in the gas phase. Table III shows that the short-time photodissociation dynamics of the A-state of diiodomethane in the solution phase have the two C-I bonds become larger by differing degrees, the I-C-I angles becomes smaller, the H-C-H angle becomes smaller and the H-C-I angles differ becomes larger. For the Franck-Condon region photodissociation dynamics, the two C-I bonds are not the same and this implies that the molecule chooses soon after photoexcitation which C-I bond undergoes cleavage. One of the reasons that the effects of solvation is very noticeable for the direct photodissociation of the A-state of diiodomethane compared to C-I bond cleavage in other iodoalkanes with only one C-I bond is that the symmetry of the two C-I bonds in diiodomethane is very sensitive to perturbation so only a small amount of solvent-solute interaction can noticeably break the symmetry of the two C-I bonds.

D. Bond Selective Electronic Excitation in Bromoiodomethane

Bromoiodomethane is an important prototype molecule for bond selective photochemistry and provides a dramatic illustration of selective bond

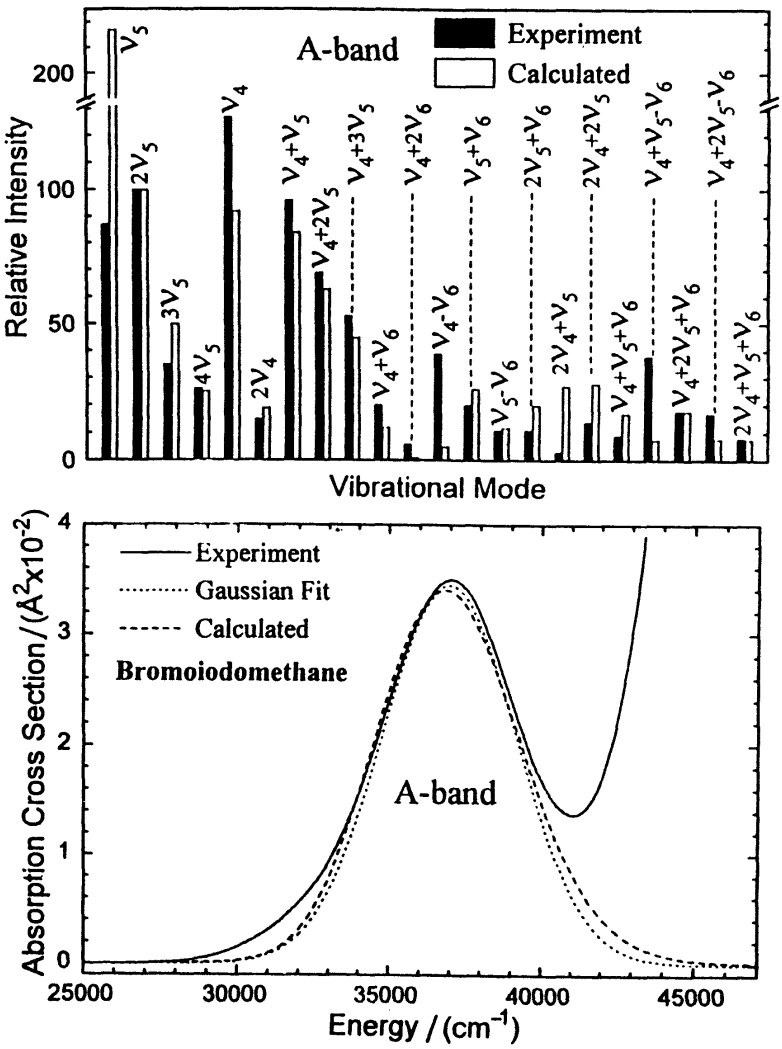

Fig. 26 Comparison of xperimental (solid bars) and calculated (open bars) resonance Raman intensities for the solution phase bromoiodomethane in cyclohexane solvent 266.0 nm resonance Raman spectrum. Comparison of the experimental (solid line), Gaussian band of the A-state deconvolution (dotted line), and calculated (dashed line) A-band absorption spectra for bromoiodomethane in cyclohexane solution. The calculations made use of the parameters and simple model given in reference [67].

cleavage by using electronic excitation of two different bonds (the C-Br and the C-I bonds).[96-98] Resonance Raman spectra were obtained including absolute Raman cross section measurements at excitation within the A-band (associated with the C-I bond) and the B-band (associated with the C-Br bond) absorptions in order to better understand the initial photodissociation dynamics associated with the bond selective electronic excitation and photochemistry. Fig. 23 shows the absorption spectra of gas and solution phase bromoiodomethane as well as bromomethane and iodomethane for comparison. Fig. 24 displays the resonance Raman spectra obtained with A-band (252.7 nm and 266.0 nm) and B-band (208.8 nm and 217.8 nm) excitation. The resonance Raman have almost all of their intensity in three Franck-Condon active vibrational modes: the nominal C-I stretch, C-Br stretch, and I-C-Br bend modes. Although the A-band and B-band have the same Franck-Condon active modes their intensity patterns are significantly different from one another and therefore their initial photodissociation dynamics are different from each other. We simulated the resonance Raman and absorption cross sections using a simple model and time dependent wavepacket calculations. Figs. 25 and 26 display comparisons of the experimental and calculated absorption spectra and resonance Raman intensities for the A-band and B-band of bromoiodomethane respectively.[67] The parameters for the best fit calculations are given in Table IV. There is reasonable agreement between the experimental and calculated absorption spectra and resonance Raman intensities shown in Figs. 25 and 26. We have obtained the short-time photodissociation dynamics in terms of internal coordinate motions associated with the A-band and B-band photodissociation reactions (we used the results of normal mode calculations in conjunction with the best fit normal mode displacements and eqs. (3) and (4)). Table IV presents the A-band and B-band short-time photodissociation dynamics at t=15 fs after photoexcitation and the diagram of bromoiodomethane shown in Fig. 27 can be used to better visualize these dynamics. Inspection of Table IV shows that the A-band initial photodissociation dynamics have the C-I bond becoming much longer, the I-C-Br angle becomes smaller, the C-Br bond becomes smaller, the H-C-I angles become smaller, the H-C-Br angles become larger, and the H-C-H angle becomes slightly smaller. The B-band short-time photodissociation dynamics show that the C-Br bond becomes much longer, the C-I bond becomes a little longer, the I-C-Br angle becomes smaller, the H-C-I angles become larger and the H-C-H angle becomes a little smaller. The short-time photodissociation

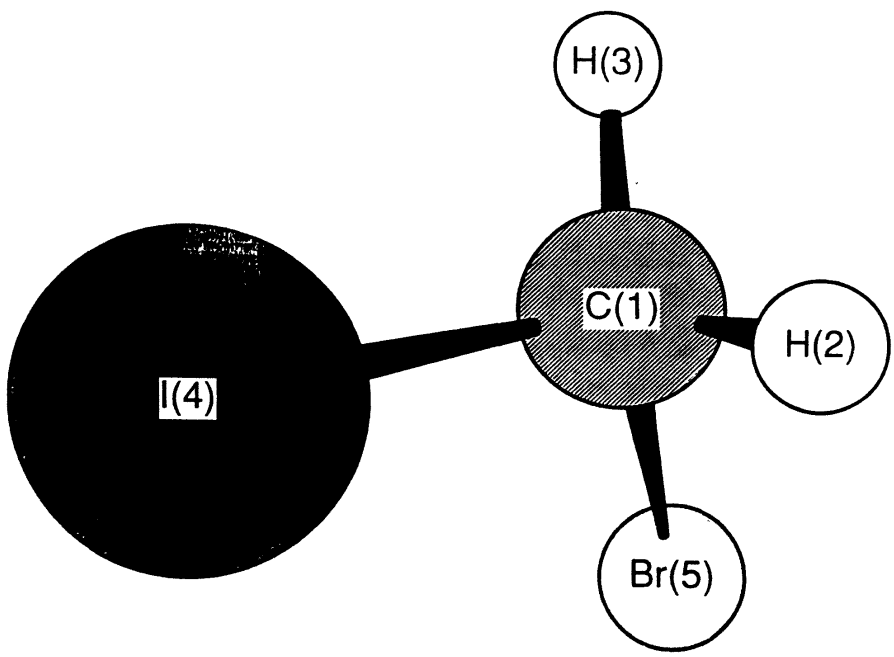

Fig. 27 Geometry of bromoiodomethane with each atom numbered 1 through 5.

Table IV

(A.) Parameters for calculation of resonance Raman intensities and absorption spectra of A-band and B-band bromoiodomethane. (B.) Most probable internal coordinate displacements of bromoiodomethane in cyclohexane solution at t = 15 fs assuming the C-I bond lengthens in the A-band and the C-Br bond lengthens in the B-band.

(A.) Simulation Parameters

A-Band Parameters

Vibrational Mode	Ground State Vibrational Frequency (cm^{-1})	Excited State Vibrational Frequency (cm^{-1})	$\|\Delta\|$
ν_4	621 cm^{-1}	621 cm^{-1}	2.65
ν_5	521 cm^{-1}	521 cm^{-1}	4.8
ν_6	151 cm^{-1}	151 cm^{-1}	4.5
Transition Length, M=0.287 Å,	E_0 = 27,200 cm^{-1},	HWHM of damping function, Γ = 50 cm^{-1}	

B-Band Parameters

Vibrational Mode	Ground State Vibrational Frequency (cm-1)	Excited State Vibrational Frequency (cm-1)	$\|\Delta\|$
ν_4	621 cm^{-1}	621 cm^{-1}	2.5
ν_5	521 cm^{-1}	521 cm^{-1}	3.0
ν_6	151 cm^{-1}	151 cm^{-1}	3.6
Transition Length, M=0.38 Å	E_0 = 41,100 cm^{-1}	HWHM of damping function, Γ = 50 cm^{-1}	

(B.) Short-Time Photodissociation Dynamics at t=15fs

		[a]Range of Displacements at t = 15 fs	
A-Band		Δ_4=-2.65	Δ_4=−2.65
Internal Coordinate	Δ_5=+4.8, Δ_6=+4.5	Δ_5=+4.8, Δ_6=−4.5	
C-H bonds	<0.01	<0.01	
C-I bond, atoms 1 and 4	+0.38	+0.37	
C-Br bond, atoms 1 and 5	−0.10	−0.10	
H-C-H angle, atoms 2, 1, and 3	−1.6	−1.4	
H-C-I angle, atoms 2, 1, and 4	−1.0	−0.4	
H-C-Br angle, atoms 2, 1, and 5	+6.5	+6.9	
H-C-I angle, atoms 3, 1, and 4	−1.0	−0.4	
H-C-Br angle, atoms 3, 1, and 5	+6.5	+6.9	
I-C-Br angle, atoms 4, 1, and 5	−9.9	−12	

		[a]Range of Displacements at t = 15 fs	
B-Band		Δ_4=+2.5	Δ_4=+2.5
Internal Coordinate	Δ_5=+3.0, Δ_6=+3.6	Δ_5=+3.0, Δ_6=−3.6	
C-H bonds	−0.01	−0.01	
C-I bond, atoms 1 and 4	+0.02	+0.01	
C-Br bond, atoms 1 and 5	+0.26	+0.26	
H-C-H angle, atoms 2, 1, and 3	−0.7	−0.5	
H-C-I angle, atoms 2, 1, and 4	+7.6	+8.1	
H-C-Br angle, atoms 2, 1, and 5	−2.7	−2.5	
H-C-I angle, atoms 3, 1, and 4	+7.6	+8.1	
H-C-Br angle, atoms 3, 1, and 5	−2.7	−2.5	
I-C-Br angle, atoms 4, 1, and 5	−8.8	−11	

[a]Values are for the two most probable sign combinations of the normal mode displacements (see ref. [67]).

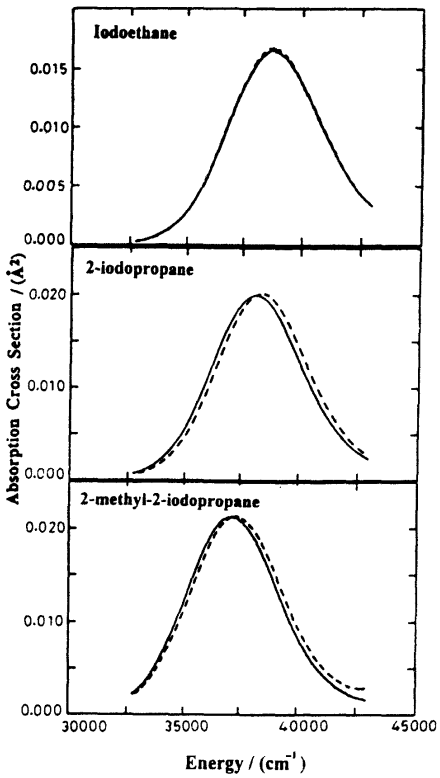

Fig. 14 Absorption spectra of iodoethane, 2-iodopropane, and 2-methyl-2-iodopropane in the gas phase (dashed line) and in cyclohexane solution (solid line). The iodoethane spectra are almost identical while the solution phase spectra of 2-iodopropane and 2-methyl-2-iodopropane are red-shifted by a small amount relative to their respective gas phase spectra.

photoproduct compared to the isopropyl and tert-butyl radicals to the degree that the short-time photodissociation dynamics can be extrapolated outside the Franck-Condon region. Our work strongly suggests that it would be very interesting to directly measure the vibrational product state distributions for the ethyl, isopropyl, and tert-butyl radicals formed from the A-band photodissociation of the corresponding parent iodoalkanes. Such studies would help generate an increased understanding of how the initial photodissociation dynamics influence the product-state energy partitioning. Several of these types of investigations have been reported for the A-band photodissociation of iodomethane to determine the vibrational-rotational state distributions of the methyl radical and applications of these types of experiments to higher iodoalkanes would likely be very rewarding.

Examination of the A-band short-time photodissociation dynamics given in Table II shows that in general there is a flattening about the α-carbon atom of the alkyl group and that the C-I bond cleavage takes place on a time-scale similar to the vibrational motions of the rest of the molecule. The results obtained by the author on resonance Raman intensity indicate that the Franck-Condon region photodissociation dynamics are somewhere between the simplistic "soft

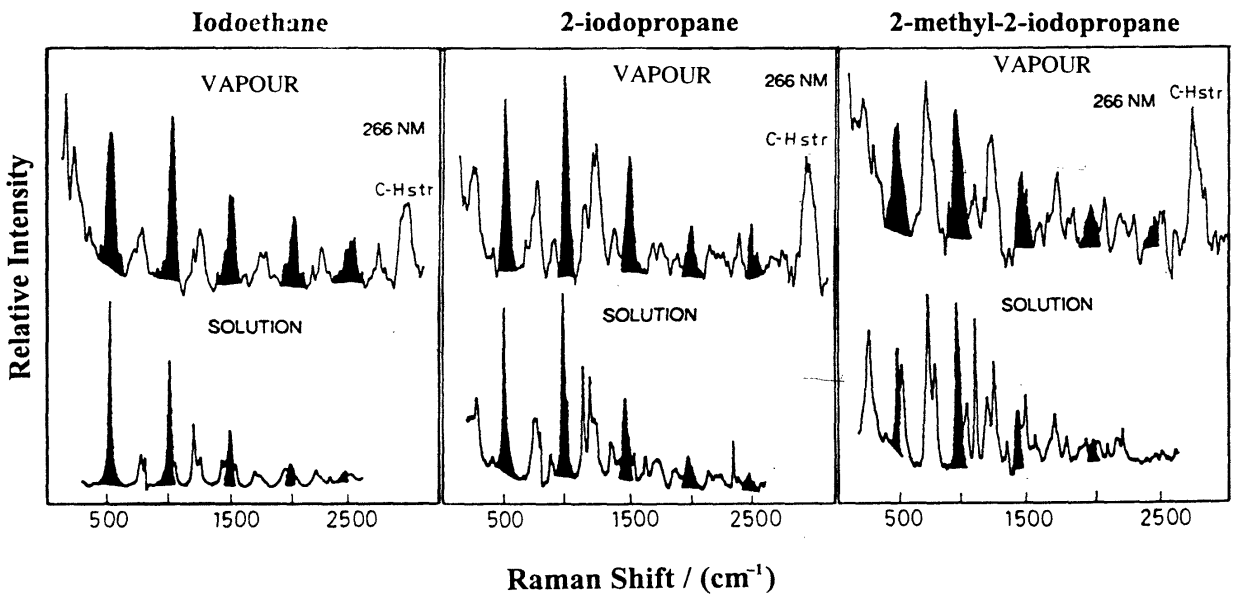

Fig. 15 Resonance Raman spectra of iodoethane, 2-iodopropane, and 2-methyl-2-iodopropane in the gas phase and in cyclohexane solution. The excitation wavelengths are all 266.0 nm except for the 2-methyl-2-iodoproane spectrum which is 268.8 nm. The gas phase spectra have instrumental resolution of 40-60 cm^{-1} while the solution phase spectra have a resolution of 8-10 cm^{-1}.

radical" and "rigid radical" descriptions of the photodissociation dynamics and that a "semi-rigid" radical model of the photodissociation dynamics would be a more appropriate description. "Semi-rigid" radical descriptions of the photodissociation dynamics could better account for the molecular bond strengths and the changes in the molecular bonds during the photodissociation process.

Comparison of the gas and solution phase iodoalkane A-band absorption and resonance Raman spectra are very similar to one another as illustrated in Figs. 14 and 15 respectively. Fig. 16 compares the gas and solution phase resonance Raman intensities for the 266 nm spectra of iodoethane, 2-iodopropane, and 2-methyl-2iodopropane shown in Fig. 15. The relative Raman intensities for the gas and solution phase spectra of the higher iodoalkanes are very similar to one another and this implies there is little solvation effect on the short-time photodissociation dynamics. This is similar to the situation in iodomethane and is not unexpected since the intramolecular forces along the reaction coordinate are much larger than solvent-solute forces in the Franc-Condon region of the A-band photodissociation. Solvation effects should become increasingly more noticeable outside the Franck-Condon region where the intramolecular forces of the photodissociation become more comparable in size to the solvent-solute forces.

C. Solvation Effects on the A-Band Photodissociation of Diiodomethane

Fig. 17 displays the ultraviolet absorption spectra of diiodomethane in the gas phase, in methanol solution, and in cyclohexane solution. The strong coupling between the two C-I chromophores causes the absorption spectra to significantly red shift relative to single chromophore iodoalkane absorption spectra as well as cause different separation and intensity in the individual transitions.[62,65,94,95] The lowest transition ~32,000 cm^{-1} forms only ground state iodine atoms while the second and higher transitions gives both ground and excited electronic states of iodine atoms.[65,94,95] The present investigation has been focused on the lowest energy transition ~32,000 cm^{-1} associated the A-state. Resonance Raman spectra (shown in Figs. 18 and 19) were obtained for diiodomethane in the gas phase (355 nm), in methanol solution (342 nm and 355 nm), and in

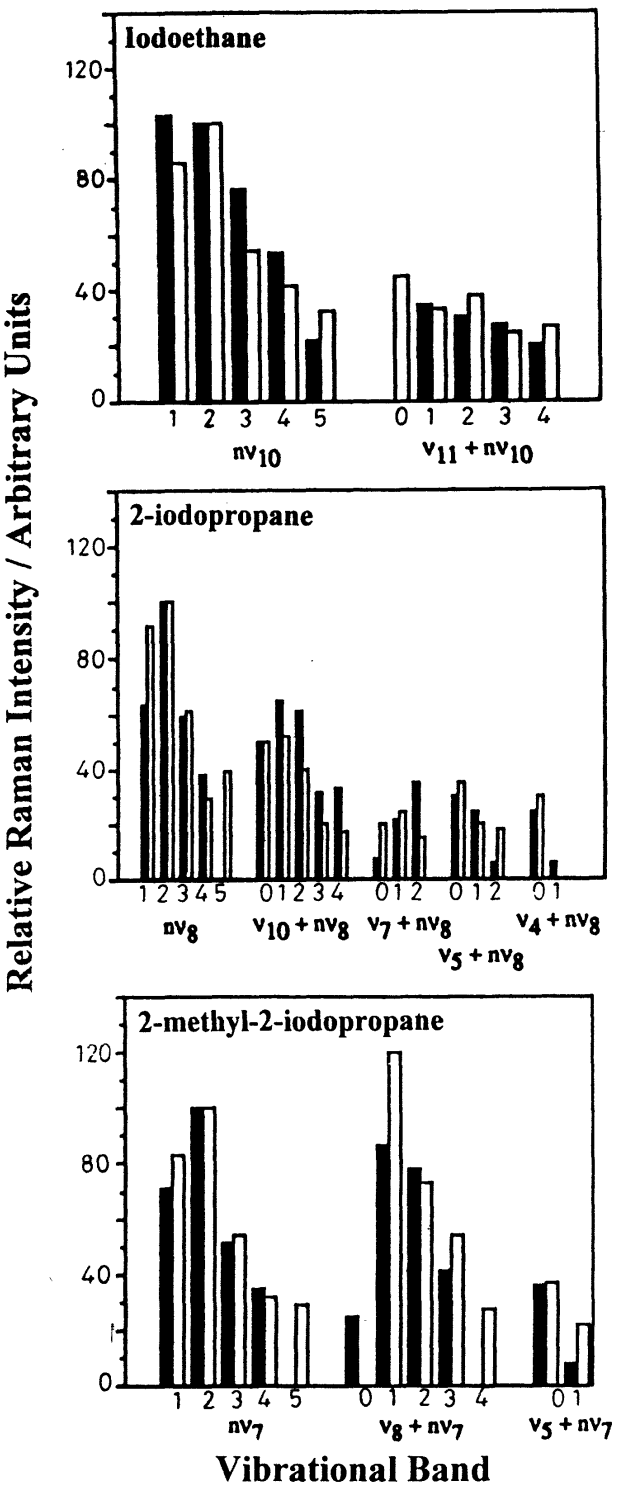

Fig. 16 Comparison of the relative Raman intensities of iodoethane, 2-iodopropane, and 2-methyl-2-iodopropane in the gas phase (open bars) and in cyclohexane solution (solid bars). Intensities of nearly degenerate bands resolved only in the solution phase have been combined as described in reference [90]. Estimated uncertainties are about ±15% for the gas phase and ±10% for cyclohexane solution.

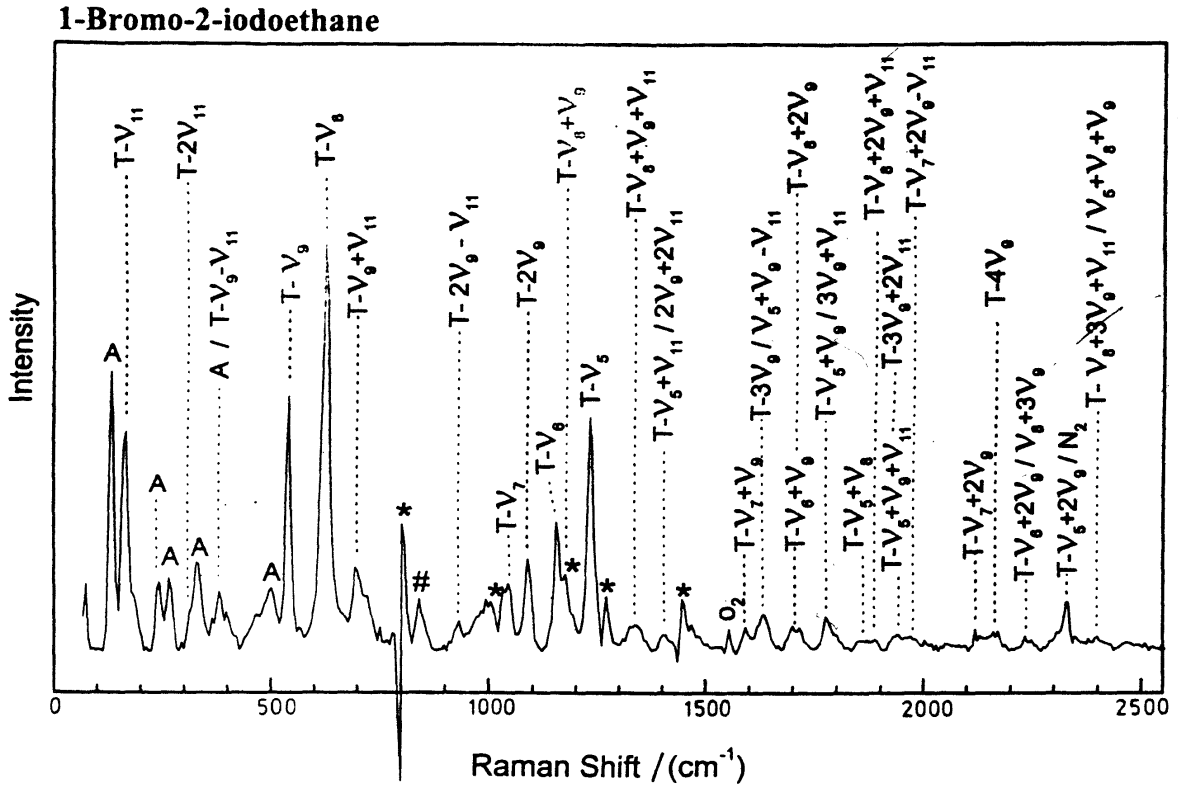

Fig. 30 Enlarged view of the 266.0 resonance Raman spectrum of 1-bromo-2-iodoethane in cyclohexane solution. The spectrum has been intensity corrected and solvent subtracted. Regions with solvent subtraction artifacts have been marked by asterisks. The more intense Raman bands have their tentative assignments displayed. The symbol A represents Raman bands due to an apparent transient species (see ref. [73]).

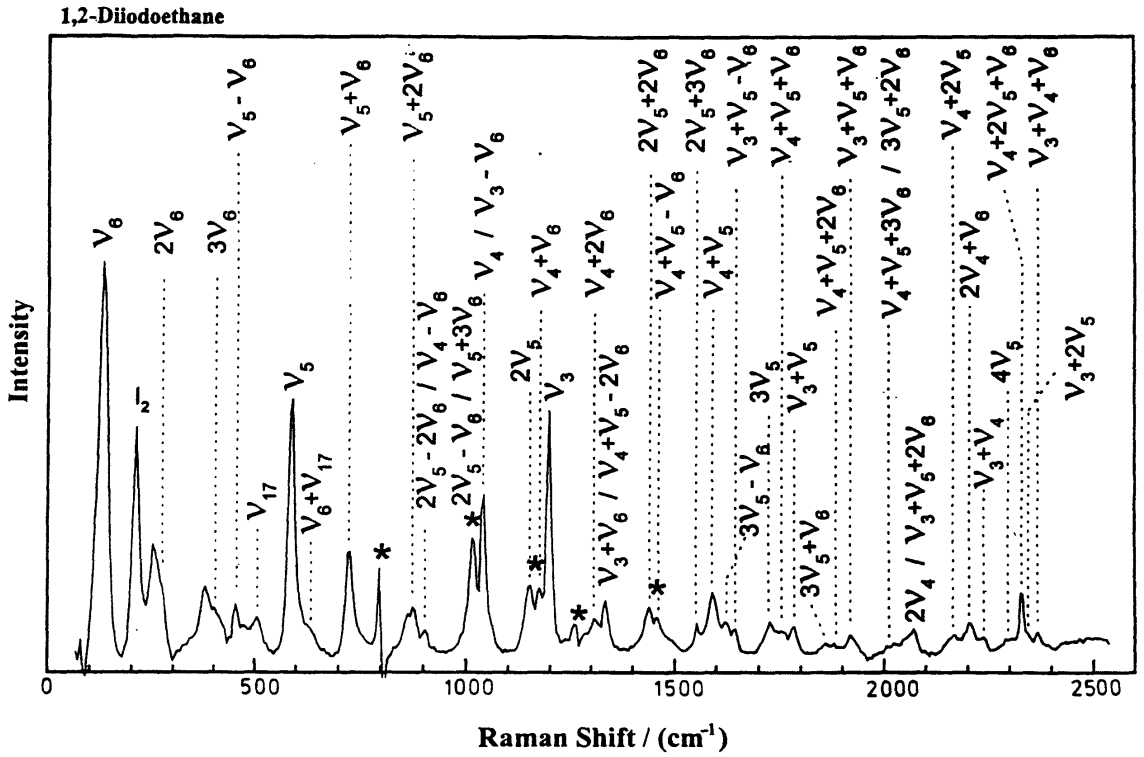

Fig. 31 Enlarged view of the 266.0 resonance Raman spectrum of 1,2-diiodoethane in cyclohexane solution. The spectrum has been intensity corrected and solvent subtracted. Regions with solvent subtraction artifacts have been marked by asterisks. The more intense Raman bands have their tentative assignments displayed.

Table V

Most probable A-band internal coordinate displacements of trans-1-bromo-2-iodoethane at t=10 fs assuming the C-I bond becomes longer and the CCI angle becomes smaller. Comparison to previous results for iodoethane, trans-1-chloroethane and trans-1,2-diiodoethane.

Trans-1-bromo-2-iodoethane (Ref. 73)

Set A (the C-Br bond becomes longer)		Set B (the C-Br becomes shorter)	
Coordinate	Range of Displacements at t=10 fs	Coordinate	Range of Displacements at t=10 fs
r_{CI}	+0.115 to +0.196 Å	r_{CI}	+0.115 to +0.196 Å
r_{CBr}	+0.013 to +0.094 Å	r_{CBr}	−0.102 to −0.021 Å
r_{BC}	−0.145 to +0.047 Å	r_{BC}	−0.115 to +0.077 Å
r_{CH}	< ±0.006 Å	r_{CH}	< ±0.006 Å
∠BCI	−11.3° to −3.3°	∠BCI	−7.6° to +0.5°
∠HCB	−10° to +11.6°	∠HCB	−11° to +10.6°
∠ICH	−8.1° to +13.6°	∠ICH	−8.8° to +12.9°
∠CBBr	−11.9° to −3.4°	∠CBBr	−8.2° to +0.2°
$\angle CBH_{7\text{ or }8}$	−11.2° to +16°	$\angle CBH_{7\text{ or }8}$	−11.3° to +14.8°
∠HCH	−1.2° to +1.9°	∠HCH	−1.6° to +1.9°
∠HBH	−1.9° to +2.5°	∠HBH	−1.8° to +2.6°
∠HBBr	−13.2° to +14.2°	∠HBBr	−13.8° to +13.6°

1-Chloro-2-Iodoethane (from Ref. 70)		Iodoethane (from Ref. 89)	
Coordinate	Range of Displacements at t=10 fs	Coordinate	Range of Displacements at t=10 fs
r_{CI}	+0.09 to +0.18 Å	r_{CI}	+0.13 to +0.15 Å
r_{CCl}	−0.01 to −0.18 Å		
r_{BC}	−0.024 to +0.012 Å	r_{BC}	−0.06 to −0.05 Å
r_{CH}	< ±0.004 Å	r_{CH}	< ±0.004 Å
∠BCI	−7.8° to +2.5°	∠BCI	−6° to −3°
∠HCB	−0.8° to +0.8°	∠HCB	+6° to +9°
∠ICH	−0.4° to +2.5°	∠ICH	−7° to −3°
∠CBCl	−8.8° to +3.2°	$\angle CBH_8$	−1° to +5°
$\angle CBH_{7\text{ or }8}$	−0.7° to +2°	$\angle CBH_{7\text{ or }6}$	−3° to −1°
∠HCH	−0.6° to +1°	∠HCH	−6° to +5°
∠HBH	−0.2° to +1.1°	$\angle H_7BH_6$	−8° to +8°
∠HBCl	−0.8° to +1.4°	$\angle H_8BH_{7\text{ or }6}$	−4° to +5°

1,2-Diiodoethane (from Ref. 72)

Coordinate	Range of Displacements at t=10 fs
first r_{CI}	+0.068 to +0.116 Å
second r_{CI}	+0.033 to +0.068 Å
r_{CC}	−0.138 to +0.071 Å
r_{CH}	< ±0.005 Å
∠CCI	−8.7° to −1.8°
∠HCC	−6.8° to +7.6°
∠ICH	−4.6° to +7.8°
∠HCH	0.0° to +2.5°

chromophore on the β-carbon atom position affects the C-I bond cleavage.[70,72,73] We have obtained a number of resonance Raman spectra at excitation wavelengths within the A-band absorptions of 1-chloro-2-iodoethane, 1-bromo-2-iodoethane and 1,2-diiodoethane in cyclohexane solutions. The absorption spectra of 1-chloro-2-iodoethane, 1-bromo-2-iodoethane and 1,2-diiodoethane in cyclohexane solution are shown in Fig. 28 and the excitation wavelengths (in nm) are indicated above each absorption spectrum. Figs. 29-31 display representative A-band resonance Raman spectra for

1-chloro-2-iodoethane, 1-bromo-2-iodoethane and 1,2-diiodoethane. The fundamentals, overtones and combinations bands of the nominal CCCl bend (ν_{10}), C-I stretch (ν_9) and C-Cl stretch (ν_8) modes account for most of the resonance Raman intensity in the A-band spectra of 1-chloro-2-iodoethane. The A-band resonance Raman spectra of 1-bromo-2-iodoethane have most of their intensity in the trans conformer fundamentals, overtones, combination bands of six Franck-Condon active

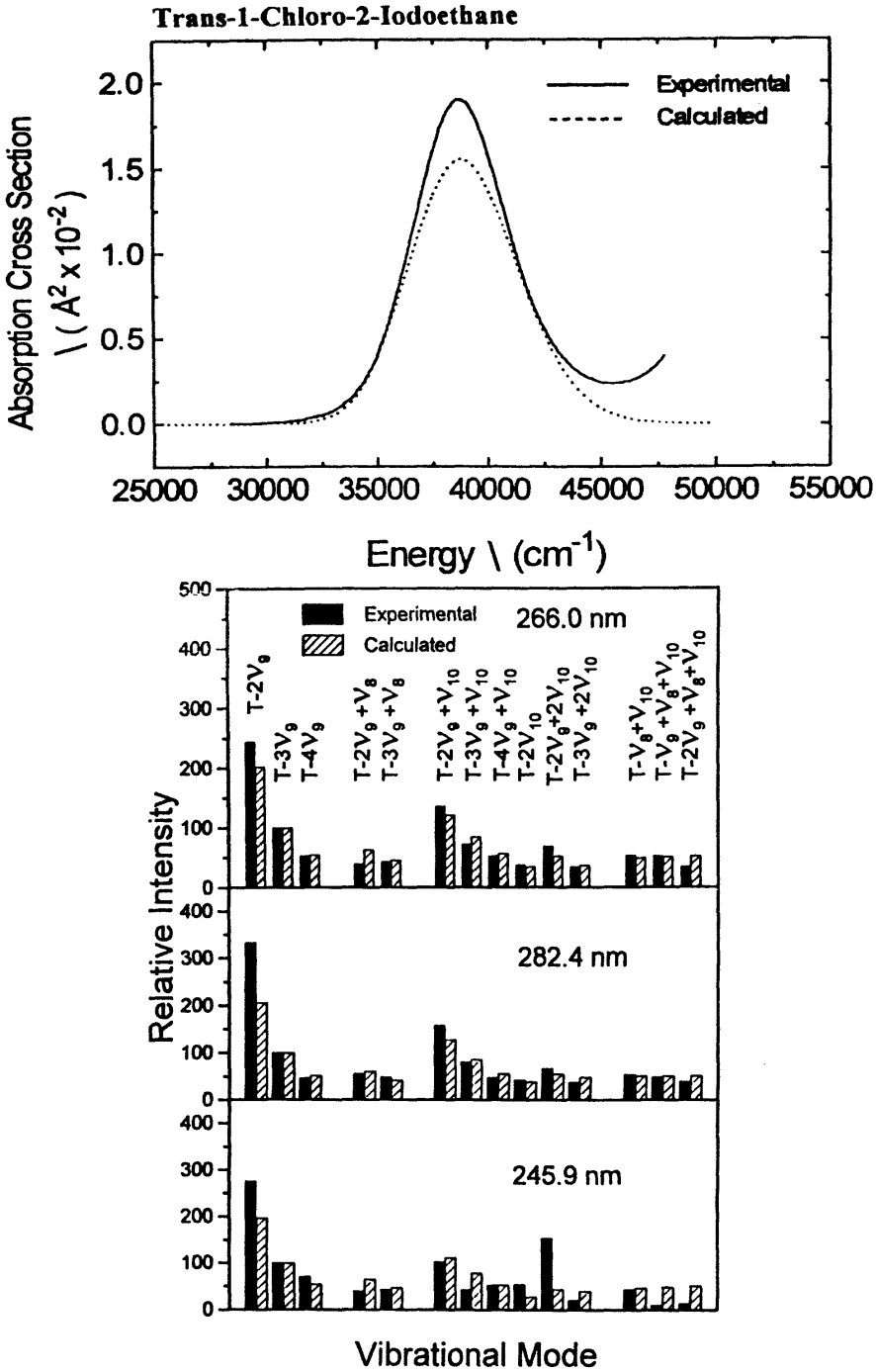

Fig. 32 Comparison of experimental (solid bars) and calculated (striped bars) resonance Raman intensities for the solution phase 1-chloro-2-iodoethane in cyclohexane solvent 266.0 nm, 282.4 nm, and 245.9 nm resonance Raman spectra. Comparison of the experimental (solid line) and calculated (dotted line) absorption spectra. The calculations made use of the parameters and simple model given in reference [70].

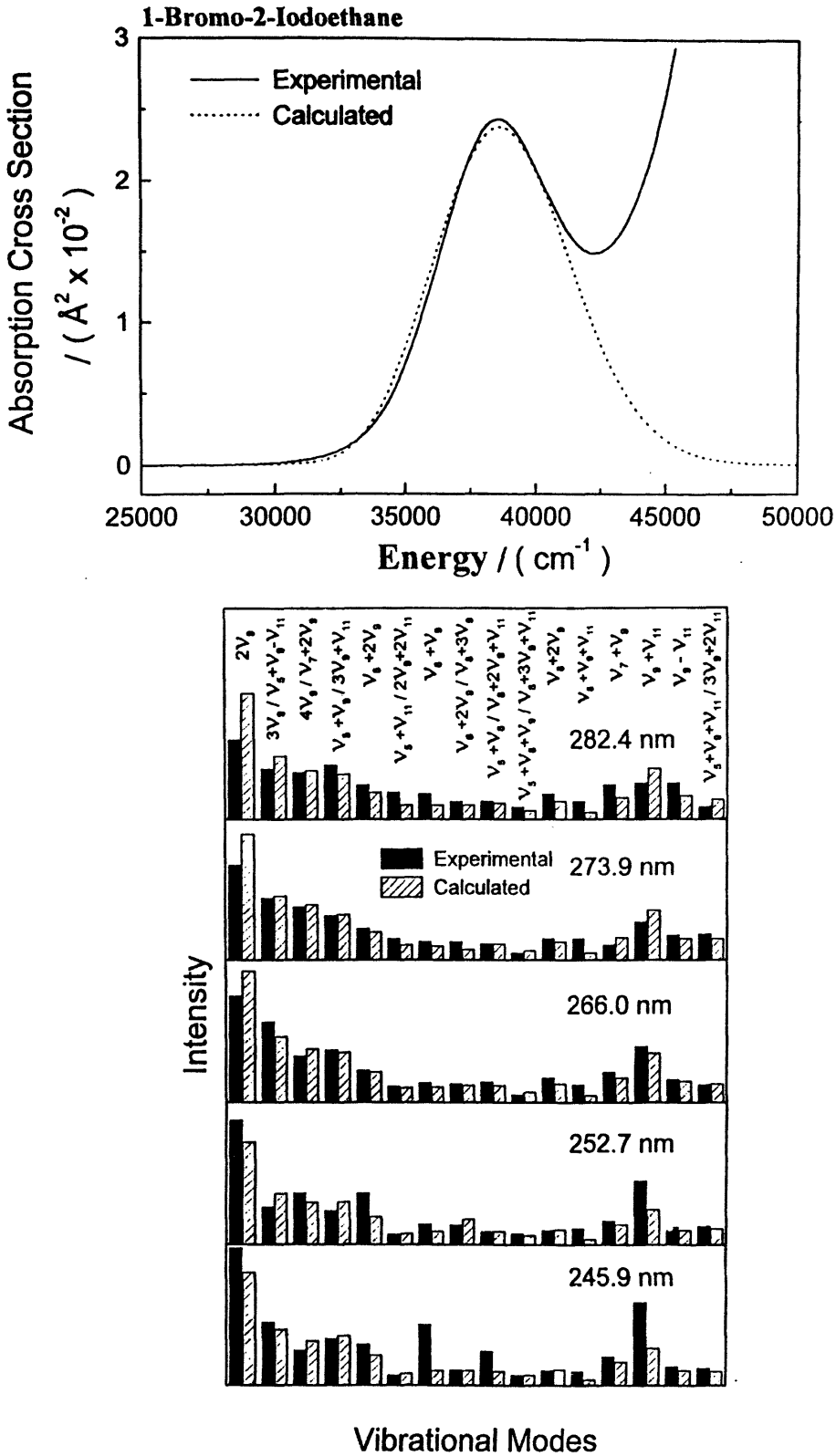

Fig. 33 Comparison of experimental (solid bars) and calculated (striped bars) resonance Raman intensities for the solution phase 1-bromo-2-iodoethane in cyclohexane solvent 282.4 nm, 273.9 nm, 266.0 nm, 252.7 nm and 245.9 nm resonance Raman spectra. Comparison of the experimental (solid line) and calculated (dotted line) absorption spectra. The calculations made use of the parameters and simple model given in reference [73].

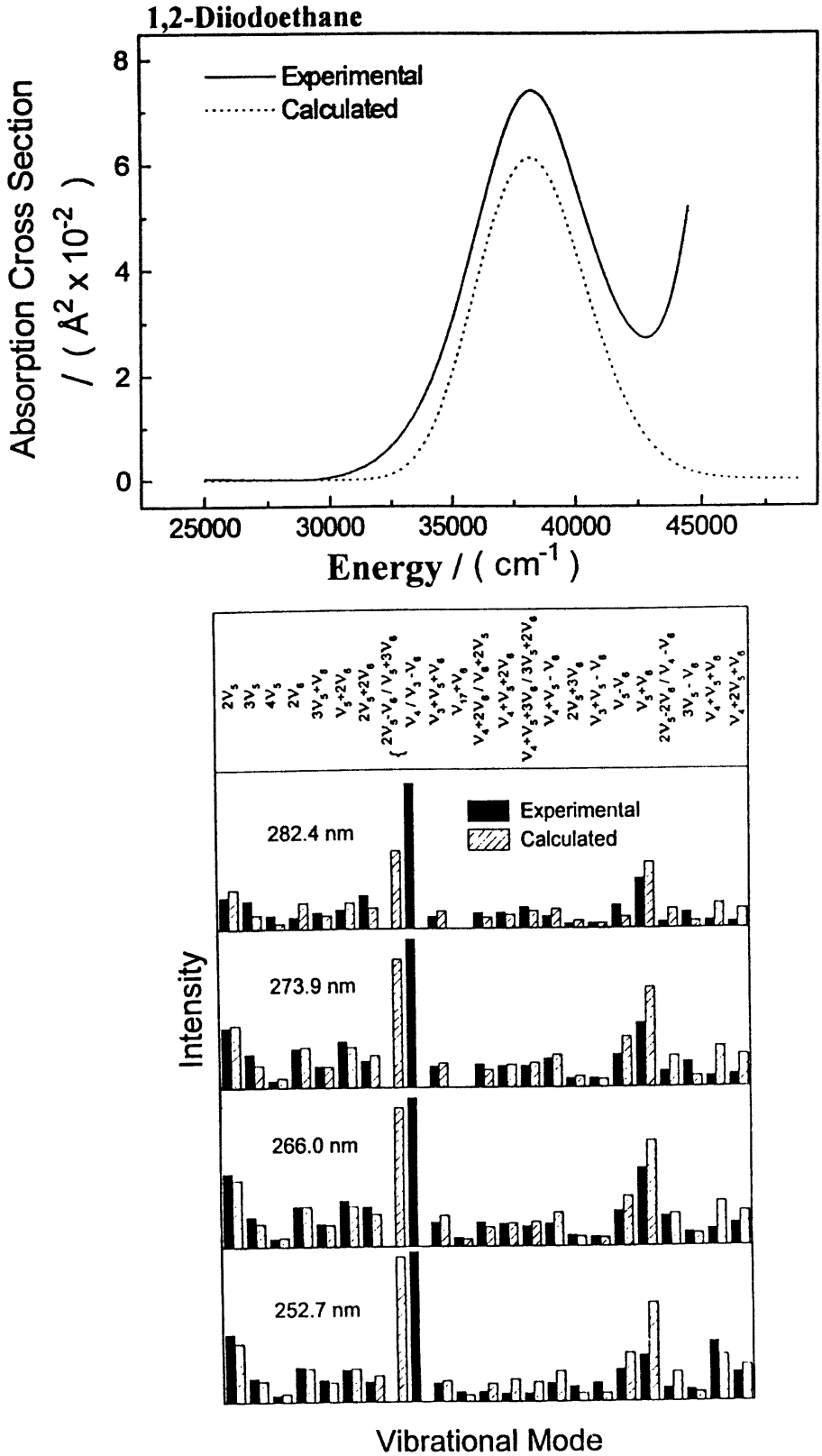

Fig 34 Comparison of experimental (solid bars) and calculated (striped bars) resonance Raman intensities for the solution phase 1,2-diiodoethane in cyclohexane solvent 282.4 nm, 273.9 nm, 266.0 nm, and 252.7 nm resonance Raman spectra. Comparison of the experimental (solid line) and calculated (dotted line) absorption spectra. The calculations made use of the parameters and simple model given in reference [72].

modes: the nominal CCI bend (ν_{11}), C-I stretch (ν_9), C-Br stretch (ν_8), C-C stretch (ν_7), CH_2 wag with the I atom attached to the CH_2 group (ν_6) and the CH_2 wag with the Br atom attached to the CH_2 group (ν_5) vibrational modes. The A-band resonance Raman spectra of diiodoethane have most of their intensity from the trans conformer fundamentals, overtones, and combination bands of five Franck-Condon active vibrational modes: the nominal CCI bend (ν_6), C-I stretch (ν_5 and ν_{17}), C-C stretch (ν_4), and CH_2 wag (ν_3) modes.

The A-band resonance Raman intensities and absorption spectra for the three 1-halo-iodoethanes were simulated using time-dependent wavepacket calculations as described in the Theory and Calculations section (and in the original publications of refs [70], [72] and [73]). Figs. 32-34 present comparisons of the experimental and calculated absorption spectra and resonance Raman intensities for 1-chloro-2-iodoethane, 1-bromo-2-iodoethane, and 1,2-diiodoethane respectively. The best fit parameters for the simulations are given in refs. [70], [72] and [73]. The experimental and calculated absorption spectra show reasonable agreement considering we are only simulating the largest $^3Q_0$ transition that accounts for most of the oscillator strength (70-90%). There is also reasonable agreement between the experimental and calculated resonance Raman intensities. The results of the best fit simulation were used in conjunction with the results of normal coordinate descriptions in order to find the short-time photodissociation dynamics in terms of easy to visualize internal coordinate changes. Table V lists the short-time photodissociation dynamics at time 10 fs after photoexcitation obtained from the

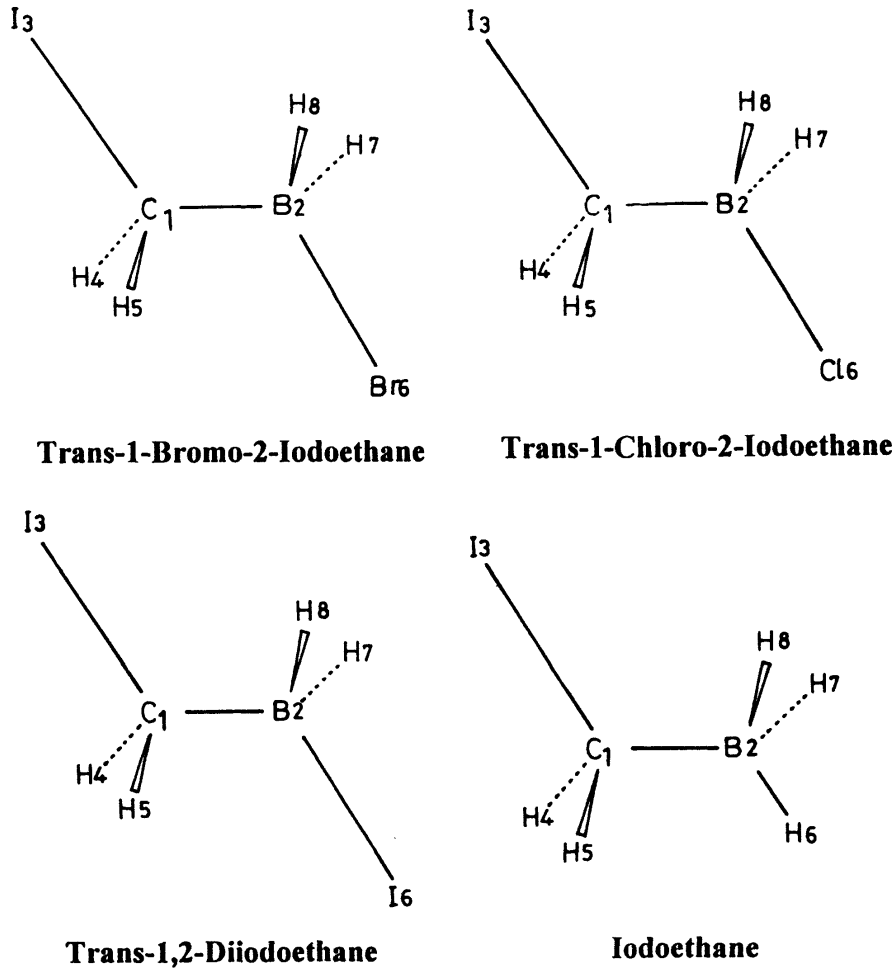

Fig. 35 Simplified geometries of the ground electronic states of trans-1-chloro-2-iodoethane, 1-bromo-2-iodoethane, and 1,2-diiodoethane which can be used to better visualize the short-time photodissociation dynamics presented in Table V.

resonance Raman intensity analysis studies done for 1-chloro-2-iodoethane, 1-bromo-2-iodoethane, and 1,2-diiodoethane. Previous results for the A-band iodoethane photodissociation are also shown in Table V for comparative purposes. Fig. 35 which displays simple diagrams of the iodoethane, 1-chloro-2-iodoethane, 1-bromo-2-iodoethane, and 1,2-diiodoethane can be used to help better visualize the short-time dynamics.

The ground state of the ethyl radical is close to a nearly planar structure and inspection of Table V shows that the initial photodissociation dynamics for the A-band of iodoethane brings the ethyl radical group closer to a planar structure and about the α-carbon atom. This suggests that there is probably little vibrational excitation of the ethyl radical photofragment in so far as the short-time dynamics translate into internal excitation of the alkyl fragment. *Ab initio* investigations indicate that the C-C bond length for iodoethane in its ground state is 1.54 Å and the C-C bond length in the ground state of the ethyl radical is 1.49 Å.[91-93] The initial photodissociation dynamics in Table V for the C-C bond length (-0.05 to –0.06 Å) brings the bond length close to that of the ground state of the ethyl radical and this also suggests that there is likely little vibrational excitation in the C-C mode of the ethyl fragment. The initial dynamics of the A-band photodissociation of iodoethane is consistent with the experimental observation that the ethyl radical photoproduct gets relatively little internal excitation (32-39% of the available energy) compared to more massive and/or branched iodoalkanes. Examination of Table V indicates that the A-band initial photodissociation dynamics of 1-chloro-2-iodoethane are significantly different from iodoethane. Both the C-I (+0.09 to +0.18 Å) and the C-Cl (-0.01 to –0.18) bond lengths at 10 fs have large displacements or range of displacements while the C-C bond length does not change much (-0.024 to +0.012 Å). The range of C-I bond displacements for 1-chloro-2-iodoethane is more similar to that of 2-iodopropane or 2-methyl-2-iodopropane which have greater internal excitation of the alkyl radical fragments than iodoethane. The initial A-band photodissociation dynamics for 1-chloro-2-iodoethane do not go toward a more planar structure about the α-carbon nearly as much as iodoethane does and this suggests that there is more internal excitation of the chloroethyl radical then the ethyl radical photoproduct (assuming the chloroethyl and ethyl radicals have a similar ground state structure-which is very likely) in so far as the Franck-Condon region dynamics determines the internal excitation of the alkyl photofragments. This is consistent with TOF photofragment spectroscopy experiments which show show a greater degree of internal excitation of the chloroethyl radical (42% to 54% of the available energy)[19,20,24,52] from 1-chloro-2-iodoethane photodissociation than the ethyl radical (32%-39% of the available energy)[99] from iodoethane photodissociation.

Comparison of the short-time photodissociation dynamics presented in Table V reveals some interesting trends. As the molecule becomes more massive, the C-I bond length changes generally proceed from a long and narrow range (such as +0.13 to +0.15 Å at 10 fs for iodoethane) to shorter and broader range (such as +0.068 to +0.116 Å and +0.033 to +0.068 Å at 10 fs for the two C-I bonds of 1,2-diiodoethane). There is also a similar trend in the C-C bond lengths (-0.05 to –0.06 Å at 10 fs for iodoethane to –0.138 to +0.071 Å at 10 fs for 1,2-diiodoethane). These trends in the C-I and C-C bond lengths for the A-band short-time photodissociation dynamics suggest that the haloethyl radical receives more internal excitation as it becomes more massive in as much as the short-time dynamics determines the photodissociation energy partitioning. This is similar to trends in the C-I bond lengths for the A-band short-time dynamics of iodoalkanes as the alkyl group becomes more massive and/or branched. The trends in the C-I and C-C bond lengths for iodoethane, 1-chloro-2iodoethane, 1-bromo-2-iodoethane, and 1,2-diiodoethane also exhibit a good correlation with time-of-flight molecular beam experimental results that indicate the available energy that goes into internal excitation of the (halo)alkyl radical product is 32%-39% for ethyl radicals from iodoethane[19,20,24,52], 42%-54% for chloroethyl radicals from 1-chloro-2-iodoethane[99], and 53%-58% for bromoethyl radicals from 1-bromo-2-iodoethane.[100]

There is one intriguing puzzle in the trends shown in Table V: The C-I bond lengths do not change much in going from 1-chloro-2-iodoethane, but the C-C bond length changes are substantially greater in 1-bromo-2-iodoethane than for 1-chloro-2-iodoethane. Why are the C-C bond length

changes so similar for 1-bromo-2-iodoethane and 1,2-diiodoethane and very different from 1-chloro-2-iodoethane? To help answer this, it is useful to examine the absorption spectral trends for the (halo)iodoethanes. The absorption coefficients for iodoethane and 1-chloro-2-iodoethane are very similar and indicate that the transitions are mainly due to the C-I bond alone. However, the absorption coefficients for 1-bromo-2-iodoethane and 1,2-diiodoethane are substantially larger and this increase in oscillator strength for the A-band absorptions cannot be simply accounted for by simple addition of the iodoethane and bromoethane absorptions for 1-bromo-2-iodoethane or two iodoethane absorptions for 1,2-diiodoethane. The observed additional increase in the A-band absorption oscillator strength for 1-bromo-2-iodoethane and 1,2-diiodoethane presumably results from significant interaction between the two carbon halogen chromophores (we note that the trans conformer accounts for most of the population in both of these molecules). Thus excitation within the A-band absorption of 1-bromo-2-iodoethane and 1,2-diiodoethane would most likely excite both the carbon halogen chromophores to some extent and this would cause the two carbon atoms of the 1,2-dihaloethanes to experience noticeable forces from both halogen atoms. Whether these forces oppose or do not oppose one another, these forces would cause additional strain on the carbon-carbon bond to give larger and broader displacements in the haloethyl group during the photodissociation. This is consistent with the initial photodissociation dynamics observed in Table V and the significantly larger C-C displacements found for the short-time photodissociation dynamics of 1-bromo-2-iodoethane and 1,2-diiodoethane is most likely due to some simultaneous photoexcitation of the carbon-halogen bonds.

Our resonance Raman studies of the dihaloethanes show that substitution of a hydrogen atom to the β-carbon of iodoethane by a more massive halogen atom leads to substantial substituent effects on the A-band short-time photodissociation dynamics. All of the dihaloethanes examined so far have multidimensional dynamics with the C-I bond cleavage occurring on a similar time scale as vibrational motion in the rest of the molecule. The initial photodissociation dynamics of the dihaloethanes are somewhere between the simple impulsive "rigid radical" and "soft radical" models of photodissociation dynamics and more similar to an impulsive "semi-rigid radical" model of the photodissociation dynamics. The dihaloethanes investigated (1-chlro-2-iodoethane, 1-bromo-2-iodoethane, and 1,2-diiodoethane) display noticeable bond length changes in the secondary carbon-halogen bond during the initial A-band photodissociation reaction arising from kinematics and/or simultaneous excitation of both C-X chromophores.

Conclusion

The resonance Raman intensity analysis studies presented here for the direct photodissociation reactions associated with excitation within the A-band absorption of polyatomic iodoalkanes and dihaloalkanes molecules show the multidimensional nature of the initial photodissociation coordinate. There is not nearly as much experimental or theoretical work done for the higher iodoalkanes and dihaloalkanes as has been done for iodomethane (the smallest iodoalkane) and this highlights the need for more experimental and theoretical work to enable a better and deeper understanding of direct polyatomic photodissociation reactions. Experiments such as magnetic circular dichroism (MCD), multiphoton ionization (MPI), femtosecond time-resolved pump-probe experiments, infrared emission and others which have been invaluable in better understanding the details of the A-band iodomethane photodissociation reaction are needed for many of the larger haloalkane and dihaloalkane molecular systems. These types of experiments and relevant theoretical investigations should enable a much higher level of understanding of the direct A-band photodissociation reactions as well as the interaction of the two C-X chromophores in dihaloalkane molecules.

Acknowledgements

The author would like to thank Professor James J Valentini and Professor Anne B Myers for many useful discussions and their encouragement. The author would also like to thank his former Ph.D. student, Dr. Wai Ming Kwok, who carried out much of the work on dihalomethanes and his

current Ph.D. student, Mr. Xuming Zheng who did much of the work on the dihaloethanes. Further, the author would also like to acknowledge his current M.Phil. student Miss Yung Fong Cheng who helped in the 1,2-diiodoethane work and Mr. King Hung Leung and Mr. Mong Yin Lau who helped to prepare the figures. Financial support from several RGC grants from the UGC of Hong Kong and CRCG grants from the University of Hong Kong are acknowledged.

References

1 E J Heller, R L Sundberg and D J Tannor *J Phys Chem* **86** (1982) 1822
2 A B Myers and R A Mathies *Biological Applications of Raman Spectroscopy* Wiley New York (1987) 1
3 R J H Clark and T J Dines *Agnew Chem Int Ed Engl* **98** (1986) 131
4 J I Zink and K S K Shin *Adv Photochem* **16** (1991) 119
5 A B Myers, *Laser Techniques in Chemistry*; Wiley: New York (1995) 325
6 B R Johnson, C Kittrell, P B Kelly and J L Kinsey *J Phys Chem* **100** (1996) 7743
7 A B Myers *Chem Rev* **96** (1996) 911
8 A B Myers, *Acc Chem Res* **30** (1997) 519
9 K Kinmura and S Nagakura *Spectrochim Acta* **17** (1961) 166
10 A Gedanken and M D Rowe *Chem Phys Lett* **34** (1975) 39
11 A Gedanken *Chem Phys Lett* **137** (1987) 462
12 T Donohue and J Wiesenfeld *Chem Phys Lett* **33** (1975) 176
13 T Donohue and J Wiesenfeld *J Chem Phys* **63** (1975) 3130
14 W H Pence, S L Baughchum and S L Leone *J Phys Chem* **85** (1981) 3844
15 P Brewer, P Das, G Ondrey and R Bersohn *J Chem Phys* **79** (1983) 720
16 W P Hess, S J Kohler, H K Haugen and S R Leone *J Chem Phys* **84** (1986) 2143
17 R Ogorzalek-Loo, G E Hall, H-P Haerri and P L Houston *J Phys Chem* **92** (1987) 5
18 F G Godwin, P A Gorry, P M Hughes, D Raybone, T M Watkinson and J C Whitehead *Chem Phys Lett* **135** (1987) 163
19 Q Zhu, J R Cao, Y Wen, J Zhang, Y Huang, W Fang, and X Wu *Chem Phys Lett* **144** (1988) 486
20 S J Riley and K R Wilson *Faraday Discuss Chem Soc* **53** (1972) 132
21 R K Sparks, K Shobatake, L R Carlson and Y T Lee *J Chem Phys* **75** (1981) 3838
22 G N A Van Veen, T Baller, A E Devries and N J A Van Veen *Chem Phys* **87** (1984) 405
23 M D Barry and P A Gorry *Mol Phys* **52** (1984) 461
24 C Paterson, F G Godwin and P A Gorry *Mol Phys* **60** (1987) 729
25 F G Godwin, C Paterson and P A Gorry *Mol Phys* **61** (1987) 827
26 J F Black and I Powis *Chem Phys* **125** (1988) 375
27 I Powis and J F Black *J Phys Chem* **93** (1989) 2461
28 R Ogorzalek-Loo, H-P Haerri, G E Hall and P L Houston *J Chem Phys* **90** (1989) 4222
29 D W Chandler, M H M Janssen, S Stolte, R N Strickland, J W Thoman, Jr and D H Parker *J Phys Chem* **94** (1990) 4839
30 N E Triggs, M Zahedi, J W Nibler, P A Debarber and J J Valentini *J Chem Phys* **96** (1992) 2756
31 G E Hall, T J Sears and J M Frye *J Chem Phys* **89** (1988) 580
32 J W G Mastenbroek, C A Taatjes, K Nauta, M H M Janssen and S Stolte *J Phys Chem* **99** (1995) 4360
33 J L Knee, L R Khundar and A H Zewail *J Chem Phys* **83** (1985) 1996
34 L R Khundar and A H Zewail *Chem Phys Lett* **142** (1987) 426
35 M Shapiro and R Bersohn *J Chem Phys* **72** (1980) 3810
36 S K Gray and M S Child *Mol Phys* **51** (1984) 189
37 M Shapiro *J Phys Chem* **90** (1986) 3644
38 M Tadjeddine, J P Flament and C Teichteil *Chem Phys* **118** (1987) 45
39 H Guo and G C Schatz *J Chem Phys* **93** (1990) 393
40 Y Amatatsu, K Morokuma and S Yabushita *J Chem Phys* **94** (1991) 4858
41 H Guo and G C Schatz *J Chem Phys* **95** (1991) 3091
42 H Guo *J Chem Phys* **96** (1992) 2731
43 A D Hammerich, U Manthe, R Kosloff, H-D Meyer and L S Cederbaum *J Chem Phys* **101** (1994) 5623
44 Y Amatatsu, S Yabushita and K Morokuma *J Chem Phys* **104** (1996) 9783
45 M K Dzvonik, S Yang and R Bersohn *J Chem Phys* **61** (1974) 4408
46 M Kawasaki, S J Lee and R Bersohn *J Chem Phys* **63** (1975) 809
47 P M Kroger, P C Demou and S J Riley *J Chem Phys* **65** (1976) 1823
48 T K Minton, P Felder, R J Brudzynski and Y T Lee *J Chem Phys* **81** (1984) 1759
49 D Krajnovitch, L J Butler and Y T Lee *J Chem Phys* **81** (1984) 3031
50 G N A Van Veen, T Baller, A E DeVries and M Shapiro *Chem Phys* **93** (1985) 277
51 Q-X Xu, K-H Jung and R B Bernstein *J Chem Phys* **89** (1988) 2099
52 W K Kang, K W Jung, D C Kim, K-H Jung and H S Kim *Chem Phys* **196** (1995) 363
53 W K Kang, K W Jung, D-C Kim and K-H Jung *J Chem Phys* **104** (1995) 5815
54 R J Donovan, F G M Hathorn and D Husain *Trans Faraday Soc* **64** (1968) 3192
55 T F Hunter, S Lunt and K S Kristjansson *J Chem Soc Faraday Trans II* **79** (1983) 303
56 E Gerck *J Chem Phys* **79** (1983) 311
57 S Uma and P K Das *Can J Chem* **72** (1994) 865
58 D H Fairbrother, K A Briggman, E Wietz and P C Stair *J Chem Phys* **101** (1994) 3787
59 P L Ross and M V Johnston *J Phys Chem* **99** (1995) 4078
60 S Uma and P K Das *Chem Phys Lett* **241** (1995) 335
61 S Uma and P K Das *J Chem Phys* **104** (1996) 4470

62 W M Kwok and DL Phillips *Chem Phys Lett* **235** (1995) 260
63 D L Phillips and W M Kwok *Chem Phys Lett* **241** (1995) 267
64 S Q Man, W M Kwok and D L Phillips *J Phys Chem* **99** (1995) 15705
65 W M Kwok and D L Phillips *J Chem Phys* **104** (1996) 2529
66 W M Kwok and D L Phillips *J Chem Phys* **104** (1996) 9816
67 S-Q Man, W M Kwok, A E Johnson and D L Phillips *J Chem Phys* **105** (1996) 5842
68 W M Kwok, P K Ng, G Z He and D L Phillips *Mol Phys* **90** (1997) 127
69 D L Phillips and A B Myers *J Raman Spectrosc* **28** (1997) 839
70 X Zheng and D L Phillips *Chem Phys Lett* **286** (1998) 79
71 X Zheng and D L Phillips *J Chem Phys* **108** (1998) 5772
72 X Zheng and D L Phillips *Chem Phys Lett* **292** (1998) 295
73 X Zheng and D L Phillips *J Chem Phys* **110** (1999) 1638
74 A B Myers, B Li and X Ci *J Chem Phys* **89** (1988) 1876
75 M O Trulson and R A Mathies *J Chem Phys* **84** (1986) 2068
76 B Li and A B Myers *J Phys Chem* **94** (1990) 4051
77 B U Curry, PhD dissertation (1983) University of California, Berkeley
78 L E Brus and V E Bondybey, *J Chem Phys* **65** (1976) 71
79 D G Imre, J L Kinsey, A Sinha and J Krenos *J Phys Chem* **88** (1984) 3956
80 M O Hale, G E Galica, S G Glogover and J L Kinsey *J Phys Chem* **90** (1986) 4997
81 G E Galica, B R Johnson, J L Kinsey and M O Hale *J Phys Chem* **95** (1991) 7994
82 K Q Lao, M D Person, P Xayaroboun and L J Butler *J Chem Phys* **92** (1990) 823
83 P G Wang and L D Ziegler *J Phys Chem* **97** (1993) 3139
84 F Markel and A B Myers *Chem Phys Lett* **167** (1990) 175
85 A B Myers and F Markel *Chem Phys* **149** (1990) 21
86 F Markel and A B Myers *J Chem Phys* **98** (1993) 21
87 D L Phillips, B A Lawrence and J J Valentini *J Phys Chem* **95** (1991) 7570
88 D L Phillips, B A Lawrence and J J Valentini *J Phys Chem* **95** (1991) 9085
89 D L Phillips and A B Myers *J Chem Phys* **95** (1991) 226
90 D L Phillips, J J Valentini and A B Myers *J Phys Chem* **96** (1992) 2039
91 J Pacansky and J Schrader *J Chem Phys* **78** (1983) 1033
92 B H Lengsfield, P E M Siegbahn and J Liu *J Chem Phys* **81** (1984) 710
93 J Pacansky, W Koch, M D Miller *J Am Chem Soc* **113** (1991) 317
94 J Zhang and D G Imre *J Chem Phys* **89** (1988) 309
95 F Duschek, M Schmitt, P Vogt, A Materny and W Kiefer *J Raman Spectrosc* **28** (1997) 445
96 S J Lee and R Bersohn *J Phys Chem* **86** (1982) 728
97 L J Butler, E J Hintsa and Y T Lee *J Chem Phys* **84** (1986) 410
98 L J Butler, E J Hintsa, S F Shane and Y T Lee *J Chem Phys* **86** (1987) 2051
99 T K Minton, G M Nathanson and Y T Lee *J Chem Phys* **86** (1984) 1991
100 G M Nathanson, T K Minton, S F Shane and Y T Lee *J Chem Phys* **90** (1990) 6157